On the Mechanism of Sparking and Finite Element Simulation of ECSM Process

A thesis Submitted
in Partial Fulfilment of the Requirements
for the degree of
MASTER OF TECHNOLOGY

by
Pulak Mohan Pandey

to the
Department of Mechanical Engineering
INDIAN INSTITUTE OF TECHNOLOGY KANPUR
March,1995

To
my
Parents

Sare Jahan Se Achchha
Hindostan Hamara

CERTIFICATE

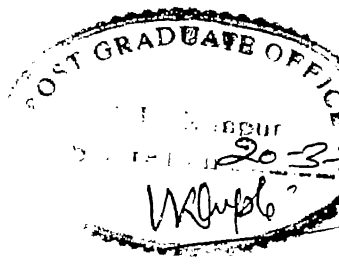

Certified that the work contained in the thesis entitled "**On the Mechanism of Sparking and Finite Element Simulation of ECSM process**", by "**Pulak Mohan Pandey**", has been carried out under our supervision and that this work has not been submitted elsewhere for a degree.

(Dr. V. K. Jain and Dr. P. M. Dixit)

Department of Mechanical Engineering,

Indian Institute of Technology,

Kanpur.

March,1995

Abstract

The advancements in today's technology need the appropriate processes for machining of low machinability materials with the desired dimensional and geometric accuracy at high rate of production and low cost. Electrochemical Machining (ECM) and Electrodischarge Machining (EDM) are the two electrically assisted nonconventional machining processes which are well established and are successfully applied in industries for the production of low machinability but electrically conducting materials. The major limitation of these processes is that only electrically conducting materials can be machined. To overcome this problem a *hybrid process* has been conceived, in which the phenomenon of Electrochemical discharge (ECD) is employed for material removal. Electrochemical Discharge is used for machining of electrically conductive work piece materials as well as nonconductive work piece materials and processes are termed as Electrochemical Arc Machining (ECAM) and Electrochemical Spark Machining (ECSM) respectively.

The *Electrochemical Spark Machining* process has been successfully applied for the machining of soda lime glass, borosilicate glass, quartz, glass fiber reinforced plastics, aramid fiber reinforced plastics and ceramics. Traveling Wire Electrochemical Spark Machining (TW-ECSM) process has dawn a new era in the field of nonconducting composite cutting and can be used for cutting composite plates in any complicated contour with the aid of numerically controlled work piece table.

The Electrochemical Spark Machining Process has been proved as a potential process to machine low machinability high strength materials, but the mechanism of the process, by and large, is not known. In the present work, the electrochemical discharge is modeled theoretically similar to the phenomenon that occurs in the *Arc Discharge Valves*. The analogous electrical circuit for the process is developed and the different experimental results have been explained on the basis of the circuit and arc discharge valve characteristics. Multivariable curve fitting technique has been used to deduce the expression for the circuit current at the time of sparking. The spark energy and the approximate order of Hydrogen gas bubble diameter have also been calculated by the proposed Valve Theory.

Material removal rate is evaluated by modeling the problem as a *3-D unsteady state heat conduction problem*. The problem is solved numerically using *finite element method* and obtained temperature distribution is post processed for the estimation of material removed

by a spark. From the isotherm plots in the workpiece domain under consideration, overcut and maximum penetration depth have also been estimated.

The conclusion drawn is that the application of valve theory for ECSM process is more realistic as compared to switching theory. Estimated material removal rate, overcut and maximum penetration depth show a good agreement with the experimental findings.

Acknowledgements

I express my gratitudes to Dr. V. K. Jain and Dr. P. M. Dixit for their valuable suggestions and perfect guidance.

I am very much thankful to Dr. V. Kulkarni of physics department, who suggested me to study the theories of discharge through gases to model the discharge phenomena.

I am also thankful to Dr. D. C. Agarwal and Dr. C. V. R. Murthy, who helped me in searching the material properties for glass.

I greatfully acknowledge CSIR for sponsoring the project entitled as " Electrochemical Spark Machining of Advanced Engineering Materials" under which this work has been carried out.

I extend my thanks to all my friends of IIT K, specially Dixitji, Sumit,Satya Prakash, and Sameer who made my stay in the institute memorable.

Pulak M. Pandey

Nomenclature

A=Constant

B=Constant

C=Constant,%**Concentration** by weight

C_p=Specific heat of workpiece material (j/kg K)

d=Depth of tool inside electrolyte (m)

E=Electric field (volt/m)

$[GC]$=Global specific heat matrix

$[GK]$=Global conductivity matrix

h=Convective heat transfer coefficient (watt/sq.m K)

I=Circuit current (ampere)

K=Conductivity of electrolyte solution (mho/m)

K_{ij}=Thermal conductivity (watt/m K)

L=Inductance (henry)

n=Constant

n_s=Number of sparks occuring simultaneously

q=Heat transfer rate (watt)

q^*=Spark energy per second (watt)

Q=Right side vector

R^*=Inherent circuit resistance (ohm)

R_b=Resistancd of valve (ohm)

R_i=Internal resistance of bulk electrlyte (ohm)

t=time (sec)

T=Temperature (K)

T_{unif}=initial Temperature of workpiece (K)

T_∞=Ambient temperature of electrolyte (K)

V=Voltage (volt)

V_b=Voltage across hydrogen bubble (volt)

V_l=Voltage induced across inductor (volt)

V_s=Supply voltage (volt)

x_i, x_j=Space coordinates (m)

α=Constant

β=Constant

γ=Constant

δ=Constant

ϕ=Diameter of tool elctrode (m)

ρ=Density of workpiece material (kg/cubic m)

Contents

List of Tables

List of Figures

Chapter 1

Introduction

1.1 Electrically Assisted Nonconventional Machining

Need of newer materials, with high strength to weight ratio and high temperature resistance, is increasing mainly with the advances in the aerospace technology. Development of such materials offers a challenge for machining of these new materials. Major difficulties in adopting the traditional machining processes for machining these materials are :

1. Low machinability,
2. Poor dimensional and geometrical accuracy, and
3. A lower rate of production and higher costs.

Hence, as a result of search for the better and faster manufacturing processes, new methods of metal cutting emerged, in which tool and workpiece do not come in physical contact like traditional machining and the processes are termed as "Nonconventional Machining processes". The nonconventional machining processes include mechanically, chemically, electrically and thermally assisted processes. Most of these processes emerged after world war II in response to the changing requirements of machining. There is a wide classification of nonconventional machining processes according to the type of energy these processes utilize. A group of unconventional machining techniques dependent on utilization of electrical energy for material removal are :

1. Electro Chemical Machining (ECM),

2. Electric Discharge Machining (EDM),

3. Electron Beam Machining (EBM), and

4. Plasma Arc Machining (PAM)

From the point of view of material removal characteristics, achievable accuracy and complex shape machining capabilities, the processes like EDM and ECM have the maximum potential. Major limitation of these processes is that only electrically conductive materials can be machined. To overcome this limitation a hybrid process is conceived which can be used for machining of electrically conducting as well as nonconducting materials. This process employs thermal energy from Electrochemical Discharge (ECD) phenomenon for material removal. The process is termed as Electrochemical Arc machining (ECAM) when used for electrically conducting workpiece material and Electrochemical Discharge (ECDM) or Electrochemical Spark (ECSM) machining when used for nonconducting workpiece materials.

1.2 Electrochemical Discharge Phenomenon

A general electrochemical cell consists of two electrodes dipped in an electrolyte as shown in Figure 1.1. Application of external potential between the electrodes causes the flow of an electric current through the cell resulting in electrochemical reaction such as anodic dissolution, plating of cathode, electrolysis etc. depending upon the electrodes-electrolyte combination. It has been observed that if two electrodes are of different sizes then beyond a certain value of applied voltage, electric sparks appear at the electrode-electrolyte interface on smaller electrode and the cell current drops. This is known as Electrochemical Discharge phenomenon.

The mechanism of Electrochemical Discharge (ECD) is not well understood. By observation of the process, it has been established that a discharge takes place due to electrical break down across the hydrogen gas bubble generated due to electrochemical reaction. According to Allesu[1] and Basak[2], the discharging is analogous to switching phenomenon of electrical switches.

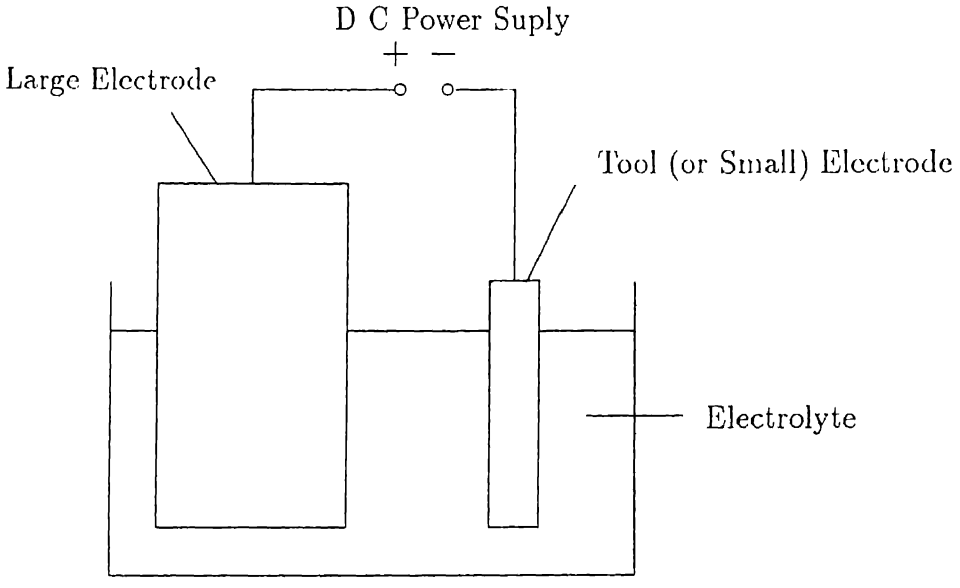

Figure 1.1: General Electrochemical Cell

1.3 Survey of Previous Work

In the recent past a large amount of experimental work has been done by researchers [7,8,1,11,12] in the field of ECSM, but the literature available in the field of theoretical analysis of ECSM process is limited.

Electrochemical spark, during electrolysis of molten NaCl at high current density, was first observed by Taylor[29]in 1925, at the anode tip and was termed as "Anode Effect". Later Kellog [13] in 1950 showed that similar phenomenon can occur at the cathode, and in aqueous electrolyte also. Electrochemical discharge between tool and work piece was also observed during the attempts for enhancing MRR in ECM by the application of higher potential between the electrodes, and was considered as detrimental factor because it damages both the tool and workpiece surfaces.

Kurafuji and Suda[15]in 1968 drilled holes upto of 0.31 mm in a glass work piece with 15 percent NaOH electrolyte and cell voltage of 34 volts. Cook et al[5] in 1973 conducted experiments with ECD for machining glass and identified the applied voltage, tool polarity, electrolyte temperature and its concentration as input parameters, for determining MRR.

Umesh Kumar [30]in 1985 also carried out the similar type of experiments but he did experiments for negative tool whereas Cook et.al [5] concentrated on positive tool. Umesh

kumar conducted experiments with flowing electrolyte and established that electric discharge vanishes with flowing electrolyte. He suggested the mechanism of material removal in ECSM process as thermo-mechanical and electrochemical actions.

Cook, Foote, Jordan and Kalyani [5] have studied the electrochemical discharge machining of glass. They found the process to be electrolyte sensitive as well as polarity sensitive. Machining rate increases both with concentration and temperature of electrolyte. Also for a given voltage the rate of machining was found to decrease with time. A pulsed DC supply was used to test the effect of high frequency pulsed current. It is found that for a pulsed power supply, with pulses in microsecond range, MRR increases by a factor of two. Surface produced by pulsed power was found to be much smoother than that from a DC power supply.

This process has been successfully applied by Tandon[27] and Rao[22] for the cutting of composite materials. Effects of voltage, electrolyte conductivity, fiber volume fraction and tool diameter on material removal rate (MRR), tool wear rate (TWR), relative tool wear rate (RTWR) and overcut have been studied by them.

Tandon[27] performed cutting of glass epoxy composites and drilling of circular blind holes in kevlar epoxy composites. He reported increase in MRR, TWR and overcut with increase in voltage and electrolyte conductivity, and also with decrease in tool diameter. It has also been reported that fiber volume fraction has no effect on TWR whereas MRR decreases slightly with increase in fiber volume fraction.

Rao[22] investigated Travelling Wire Electrochemical Spark Machining (TW-ECSM) of composites. He reported similar effects of voltage on MRR, TWR and overcut as reported by Tandon[27]. Increase in NaOH concentration, increases MRR, TWR and overcut upto 20 percent concentration. Beyond this concentration the values of these responses decrease, primarily because the value of specific conductance beyond approximately 20% concentration decreases. Effect of bubbles on ECSM process was also studied by introducing artificially produced bubbles. It resulted in lower MRR because most of the bubbles died out without sparking. However, accuracy of the machined component was found to be better.

Tsuchiya et al[28] used wire electrochemical discharge for machining of glass and ceramics. The cutting technique of wire-EDM was combined with ECSM. They used 25 Hertz rectangular pulse frequency with 80 percent duty factor, NaOH and KOH as electrolyte, ceramic specimens, and copper wire as electrode (tool) travelling with speed of 60 cm/s.

Mc Geough and Crichton[4] have reported from the observations made using high speed photography, that both spark and arc discharges are possible in an electrolyte. According to them one of the following three phenomena would take place when the voltage is applied across the two electrodes immersed in the electrolyte :

1. Electrochemical action only,
2. Electrochemical action followed by discharge between electrode and electrolyte, and
3. Electrochemical action followed by discharge between the electrodes.

Allesu [1] conducted experiments to study both ECD phenomenon and ECDM process. The suggested mechanism of material removal depends on electrochemical action, thermal erosion and cavitation. A lot of observations, such as the limited depth characteristics, shifting of the discharge zone due to penetration of the tool inside the workpiece and melting of tool (cathode) at high voltage were made. Microwelding of two different type of material wire for thermocouple bead and engraving on glass are two major achievements of his work[9]. He reported the distribution of voltage drop in an ECDM bath, which was later on verified by Basak[2].

Basak [2] carried out extensive experiments on the machining of glass using ECSM process with different electrolytes such as NaOH, KOH and NaCl and with different type of power supply like smooth DC and 100 hertz full wave rectified DC. Effect of inductance on the external circuit was also studied and it was concluded that with an increase in inductance of the circuit the MRR increases. He carried out experiments by varying inter-electrode gap and electrode size, and concluded that the electrode size affects the V-I characteristics of the circuit but interelectrode gap does not show a significant effect on the process parameters. On the basis of Paschen's Curve from electric contact theory was found that the minimum voltage for breakdown through bimolecular gas is of the order of 250 volts. He developed a theoretical model of the process based on switching phenomenon of electrical switches. By analogous electrical circuit of the process, he calculated discharge energy and by using semi-infinite material domain the material removed by a single spark was estimated. With the help of frequency of sparking, based on discharge time for switching action, material removal rate has been calculated which shows a good agreement with the experimental results. The theory also predicts the critical discharge voltage and current.

1.4 Switching Theory of Sparking in ECSM Process

1.4.1 Switching Theory[2]

In ECM process, hydrogen is liberated and gets accumulated at the cathode(tool). The bubble density at the tool is responsible for initiation of discharging. The bubble density at the tool increases with an increase in supply voltage as the rate of electrochemical reaction is proportional to supply voltage. When the nucleation site density of the hydrogen gas bubbles becomes sufficiently high, substantial constriction of the current path takes place at the interface of the tool and electrolyte. The constriction causes an increase in the resistance at the region and ohmic heating of electrolyte solution becomes significant. This causes the onset of vapour bubble nucleation on the electrode surface in addition to the hydrogen bubbles. Beyond this stage the number of the combined nucleation sites increases very rapidly with the applied voltage. As the nucleation site density reaches a critical value, vapour blanketing of the electrode occurs. At this stage maximum coverage of electrode surface inside the electrolyte takes place with fully grown hemispherical bubbles. The points of contact between the electrolyte and the tool, known as "bubble bridge", blows off instantly due to intense heating. Consequently the current through the circuit drops to zero within a very short time span which is analogous to switching off in an electrical circuit. Discharge takes place along the location of the bubble bridge (Figure 1.2). The spark energy is released and utilized for cutting workpiece materials. The bubbles get dislodged from the electrode surface due to bridge blowing and the contact between the electrode and the electrolyte is reestablished. The cycle repeats continuously.

1.4.2 Comments of Author on Switching Theory

1. The basis of switching theory is "Paschen's Curve", which is valid[14] for the case of *Townsend Discharge*. Townsend discharges are those electrical discharges through gases which commence when the absolute pressure of gas in the discharge tube is of the order of few mm of mercury. The current ranges in micro amperes. In ECSM process, the tool is dipped only about 2.0 mm inside the electrolyte and the electrolyte remains exposed to the atmosphere therefore the order of pressure inside the liberated gas bubbles is approximately atmospheric. The current in ECSM process has

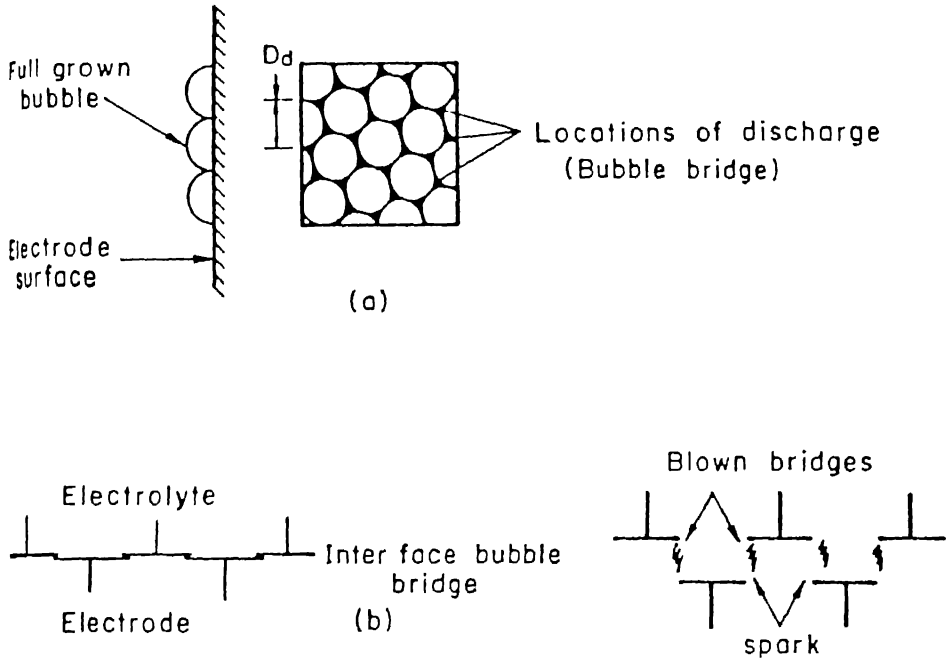

Figure 1.2: Idealization for Bubble Bridges[2]

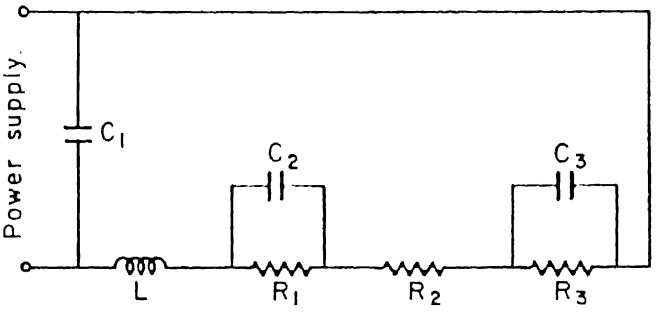

Figure 1.3: Equivalent Circuit of ECSM process (Switching Theory)

been reported upto 1.5 ampere [1, 2], which is much higher than the current range prescribed for the townsend discharges.

2. The bubbles accumulate on the tool (cathode) and at critical condition when the dipped portion of the cathode is completely covered by the bubbles, the current flows only through the bubble bridges which offer high resistance in the path of the electric current, therefore the ohmic heating of the electrolytes at these sites starts, and may result in vaporization of the electrolyte. If it is heated beyond this stage then the temperature of this mixture of hydrogen and vapour will increase and the size of the bubbles will increase due to expansion of gas. Therefore the bubbles get dislodged from the electrolyte due to increased buoyancy force. The bubble bridge can not blow because any liquid which can not be fired never blows, and it is contradictory to what is indicated in the switching theory.

3. According to the switching theory, vapour blanketing of the tool occurs, which implies that there will not be bubble bridge at the critical accumulation condition of the bubbles. Similar type of phenomenon is observed in primary cells where a cell stops supplying power after some time, because of complete accumulation of bubbles on the cathode. This event is called polarization of cell.

4. The equivalent circuit of the process in this theory is shown in Figure 1.3.

   In a DC supply only resistance is the inherent characteristic of the circuit. C_2 and C_3 are taken as capacitors parallel to the electrodes. Capacitive effects may induce due to *electrode potential effect*, when circuit is open and at that time opposite charges

exist in electrode and electrolyte at finite distances. Theyare called half cells and do not exist when the circuit is closed.

Only one of the resistance in R_1 and R_3 (resistance induced due to accumulation of hydrogen bubbles on electrodes) should be considered because at unique condition of set up, only one electrode is critically accumulated with bubbles. Therefore the resistance corresponding to electrode which is uncovered with bubbles is very small and can be neglected.

Effect of L (inductance) comes into picture even in DC circuit, because current is not constant during sparking and

$$V_L = -L\frac{dI}{dt} \tag{1.1}$$

where V_L = Voltage induced across inductor.

I = Circuit current

t = time

5. The equivalent circuit of the process does not explain the voltage distribution in ECSM bath as observed by Allesu[1] and Basak[2].

6. The theory does not throw light on the reasons for the metallic sound and glowing (lightening) during sparking.

7. In switching of electrical switches the current drops to zero, but in the process current never drops to zero as it is observed experimentally on oscilloscope [2].

1.5 Objective and Scope of the Present Work

The literature survey indicates that ECSM process can be successfully applied for the machining of glass, composites, and ceramics. However the mechanism of material removal during the process and the phenomenon of electrochemical discharges is yet not clear. The model available for quantitative estimation of MRR does not seem to be realistic. Therefore the main objectives of the present thesis work are:

* To identify ECD phenomenon.

* To develop simple and realistic quantitative model capable of predicting the material removal rate.

* To find out overall efficiency of the process.

The mechanism of electrochemical spark machining and electrochemical discharge is quite complicated and is due to many interdependent phenomena like discharges through gases, electrochemical reactions, boiling phenomenon and cavitation effects. In the present work, the electrochemical discharge phenomena is considered analogous to the discharge phenomenon that occurs in the arc discharge valve. On the basis of arc valve characteristics *Valve Theory of ECSM process* has been proposed. A multivariable curve fitting technique has been used in order to obtain expressions for circuit current during sparking.

The problem for MRR evaluation is formulated as 3 D unsteady state heat conduction problem with Neumann and Robbins boundary conditions. The location of the heat source (spark) is determined with the help of random number generation. The variations in material properties with the temperature have been considered. Finite Element Method has been employed to get temperature distribution in the workpiece. Material removed per spark has been calculated by the volume of material above the softening temperature of the workpiece material. Material removal rate is obtained by the average material removed over the number of sparks required for sweeping one layer of the material, multiplied by the number of sparks in one minute.

Chapter 2

Application of Valve Theory for ECSM Process

A new theory for ECSM process has been proposed and discussed in this chapter. The theory is based on the theory of discharge through gases. Different assumptions are made to idealize the process according to gas discharge theory and thus equivalent circuit for the process is developed. The spark energy has been calculated on the basis of the developed circuit.

2.1 Discharge Through Gases

Flow of electric current through gaseous medium is known as discharging through gases. During the course of flow of electric current through gases, the gas gets ionized and the means of ionization may be thermal energy, electric field or photons and accordingly, the emissions are termed as thermal emission, field emission and photo electric emission respectively.

There are three types of discharge through gases (refer Figure 2.1) :

2.1.1 Townsend Discharge

Townsend discharge is invisible, because the atoms which emit visible light are small in number. It is not a self sustained discharge and requires external agency to produce electrons either in gas itself or from negative electrode. The agency may be ultraviolet rays, x-rays

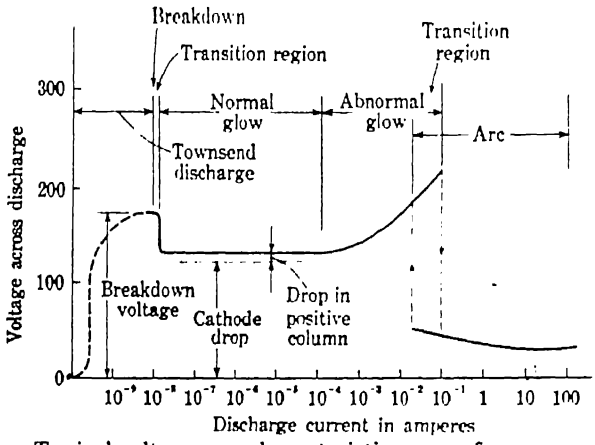

Typical volt-ampere characteristic curve of a gaseous discharge through the Townsend, glow, and arc regions.

Figure 2.1: V-I characteristics of a Discharge Tube[**14**]

or cosmic rays. The absolute pressure of gas is of the order of few millimeter of mercury, and voltage ranges above 100 volts. The current is not more than 10^{-6} ampere.

2.1.2 Glow Discharge

If the voltage across the tube having townsend discharge is increased, after a certain voltage the current increases sharply by several order of magnitude. This is the breakdown point and the voltage ranges from 200 to 300 volts depending upon the pressure, nature of gas and separation of electrodes. Once breakdown has occurred the discharge becomes self sustaining and takes a form of glow or an arc discharge depending upon the gas pressure and circuit conditions.

In either case, the gas becomes luminous. The current ranges from 10^{-6} to 10^{-1} ampere.

2.1.3 Arc Discharge

If pressure of the gas inside a tube is nearer to the atmospheric and the resistance of external circuit is low, the breakdown results in an arc discharge. This discharge is intensely luminous and may give the impression of violent turbulence. Current in the circuit is determined by

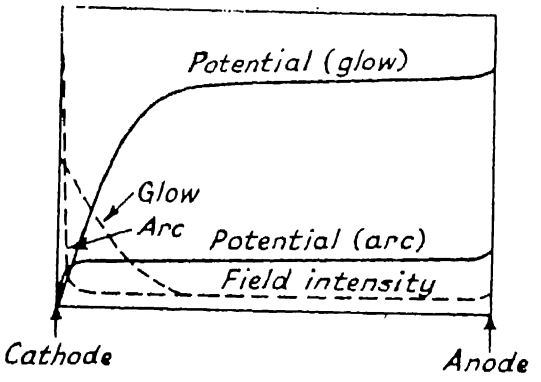

Figure 2.2: Variation of Potential along Arc Discharge[14]

external circuit parameters and voltage across the discharge is low, usually some tens of volts.

The order of electric field required is 10^6 volt per meter. It is not necessary that high value of electric field can be produced only by very high discharge voltage. Intense electric field can be produced by space charge over very short distance in low voltage discharges. It is particularly true when the cathode surface is partly covered with insulating particles. The arc discharge is characterized by a higher current and a much lower voltage than the glow discharge. The arc discharge voltage is typically less than 50 volts, and it is approximately 13.2 volts at atmospheric gas pressure. At high pressures of the order of one atmosphere, the arc appears to have an intense core with no discermible structure and outer regions like a hot flame. The variation of potential along arc discharge is indicated in Figure 2.2. The Figure 2.2 indicates that the voltage fall region near the cathode is very narrower, of the order of a fraction of mm .

2.2 Application of the Valve Theory for Sparking in ECSM process

The above discussion on discharge through gases helps in concluding that the arc discharge occurs through hydrogen gas bubble during ECSM process because the order of pressure of hydrogen inside the bubble is approximately atmospheric. It is due to the fact that bubbles are only few mm deeper inside the electrolyte. Further the circuit current ranges from 0.1 to 1.5 ampere and the supply voltage usually varies from 30 to 60 volts. These conditions lead to conclude that the sparking during ECSM process is result of arc discharges.

Following assumptions are made so that the arc discharge valve theory can be employed to idealize the ECSM process.

2.2.1 Assumptions

1. It is assumed that the arc discharge takes place through hydrogen bubbles at the electrode surface and the discharge energy is responsible for the removal of material from the electrically nonconducting workpiece.

2. As the supply voltage increases the rate of electrochemical reaction also increases. Therefore hydrogen bubbles may increase in number and also grow in size. It is obvious that bigger bubble can not sustain discharge for as long as a smaller bubble can. Therefore the frequency of sparking is not independent of supply voltage. In this model the frequency of sparking is assumed to be constant at 2000 hertz. Assuming that there is no overlap between two sparks the discharging time is taken as 0.0005 sec, as indicated in spectrograph obtained by Basak [2] (Figure 2.3).

3. As the discharge takes place across a hydrogen bubble it collapses, and the bubbles surrounding this bubble also collapse. Immediately, the space is occupied by other bubbles. Thus for a moment a small current flows through the bubble bridges. At micro level (as observed by Basak on CRO and Spectroscope) the current does not remain constant but fluctuates with time and gives rise to an inductive effect to the circuit. In the present work, inductive effect is assumed to have insignificant effect on the process.

4. The chemical reaction is also possible at very high temperatures, which is not considered in the present work.

5. The radiation losses to the electrolyte and atmosphere are neglected.

6. Heat loss due to conduction to the anode is neglected.

2.3 Equivalent Circuits for the Process

On the basis of the assumptions made in the previous section, and using the concepts of electrical circuits and characteristics of ECSM process, the equivalent circuits for the process

Figure 2.3: Wave Shape of Current at the time of Sparking

have been developed and discussed below :

The equivalent circuit of the process at the time when there is no sparking is shown in Figure 2.4a where R^* is inherent circuit resistance, which includes resistance of connection wires and other contact resistances. R_i is internal resistance of the bulk electrolyte. The equivalent circuit of the process when the tool is critically covered with hydrogen bubbles (but no sparking) is shown in Figure 2.4b. The circuit includes the resistances (R_b of each bubble in parallel) analogous to the arc discharge valves (H_2 gas bubbles). Figure 2.4c includes inductance in series and has a meaning when there is discharging. Hydrogen bubbles collapse and there is a change in the circuit current and hence inductive effect induces in the circuit.

Inductor (L) stores energy when there is increase in circuit current and releases energy when current decreases. The action of an inductor is similar to a flywheel in the reciprocating engine. Thus inductive effect works in keeping circuit current at constant values. As the circuit current variation is observed at micro level therefore in this study inductor is removed from the circuit.

Therefore, for the calculation of discharge energy of a spark, the idealized circuit is shown in Figure 2.4d. The procedure for calculation of spark energy is described in the next section.

2.4 Calculation of Energy Released per second by a Spark

At the time of sparking and collapsing of bubbles the energy supplied per second by the D C supply source is consumed (Figure 2.4d) in the following events :

1. Joul's heating of electrolyte (I^2R_i),
2. Inherent losses in the circuit and contacts (I^2R^*),
3. Losses at bubble contacts, and
4. Productive energy, that is discharge energy through valves (or hydrogen gas bubbles).

Therefore,

productive energy per second = Energy supplied by D C source per second - Energy lost in non-productive events

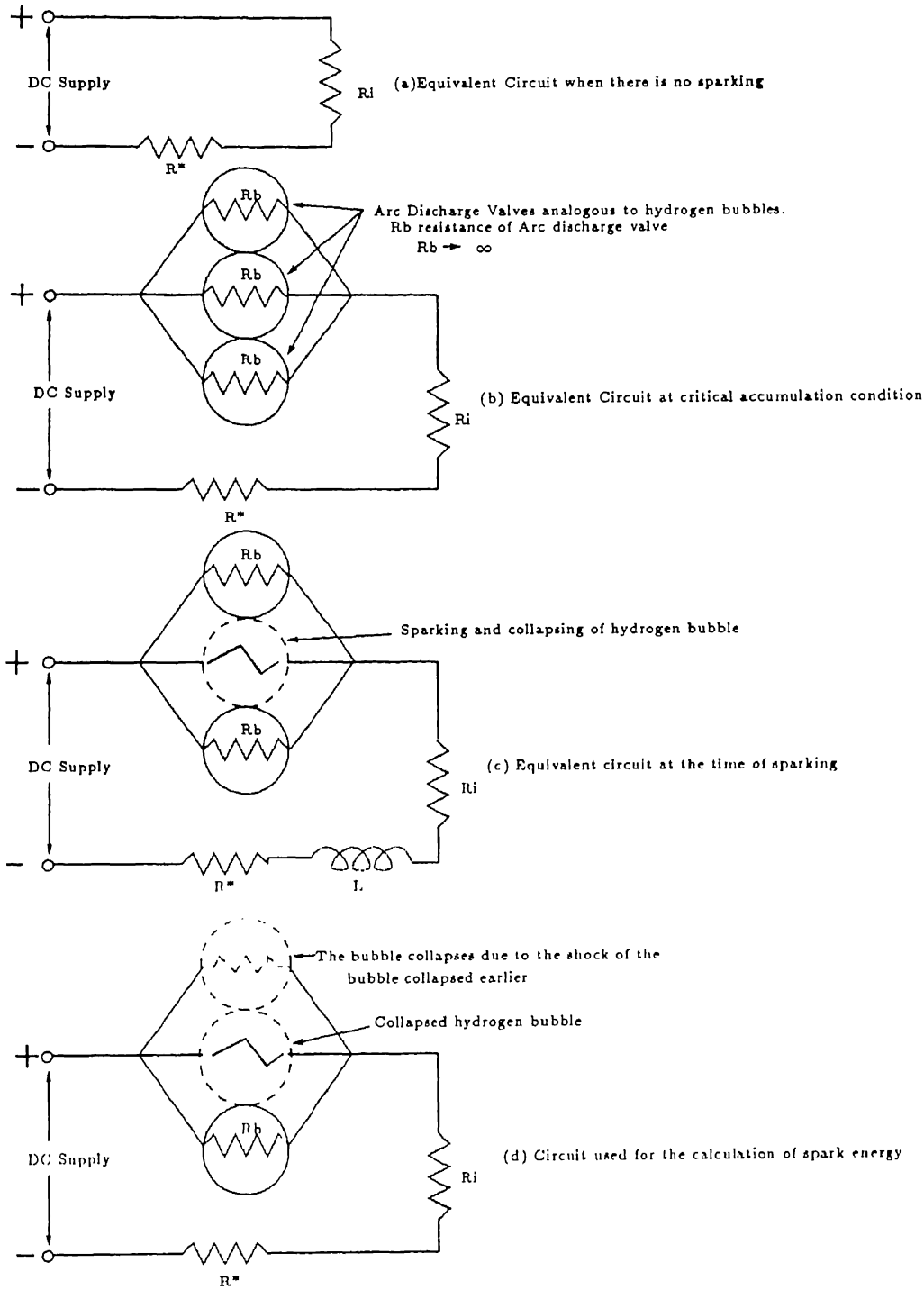

(Note : Only Three bubbles are shown in the Figure, although there are number of buubles which are to be considered in parallel to main supply.)

Figure 2.4: Equivalent Circuits for ECSM process

$$= V_s I - I^2 R_i - I^2 R^*$$

where, V_s is supply voltage, I is circuit current, R_i is internal resistance of the bulk electrolyte and R^* is inherent circuit resistance.

Neglecting R^*, energy released by sparks per second is given by

$$q^* = (V_s I - I^2 R_i)/N_s \tag{2.1}$$

Expression for circuit current (I) at the time of sparking is derived in next section.

Where the number of sparks occurring simultaneously is N_s, however the value of N_s has been taken as 1 in the present work.

2.5 Calculation of Circuit Current at the time of sparking

The voltage current relationship for arc discharge valves [21],

$$V = A + BI^{-n} \tag{2.2}$$

where A, B and n are constants. The values of A and B depend on the arc length and the value of n depends on the boiling temperature of the anode.

The values of A and B for 3 mm arc length are 29.0 and 37.0 respectively. The values of n for copper and carbon as anode are 0.67 and 1.0 respectively. Two graphs showing V-I characteristics using these data have been drawn for n=1 and n=0.67 shown in Figure 2.5a and Figure 2.5b respectively. The range of current and its trend of variation with voltage matches with that obtained during actual ECSM process [2] as shown in Figure 2.6.

In ECSM process, circuit current during sparking is a function of many parameters in which supply voltage, electrolytic conductivity, tool diameter and depth of tool inside electrolyte are the most important [2]. Therefore it was decided to fit a curve of the type $Y = Cx_1{}^{\alpha}x_2{}^{\beta}.....$ in order to evaluate the effect of various independent (x_1,x_2,..., on the response r) simultaneously.

Circuit current at the time of sparking is represented by Equation(2.3)

$$I = f(Vs, K, \phi, d) \tag{2.3}$$

or,

$$I = CV_s{}^{\alpha}K^{\beta}\phi^{\gamma}d^{\delta} \tag{2.4}$$

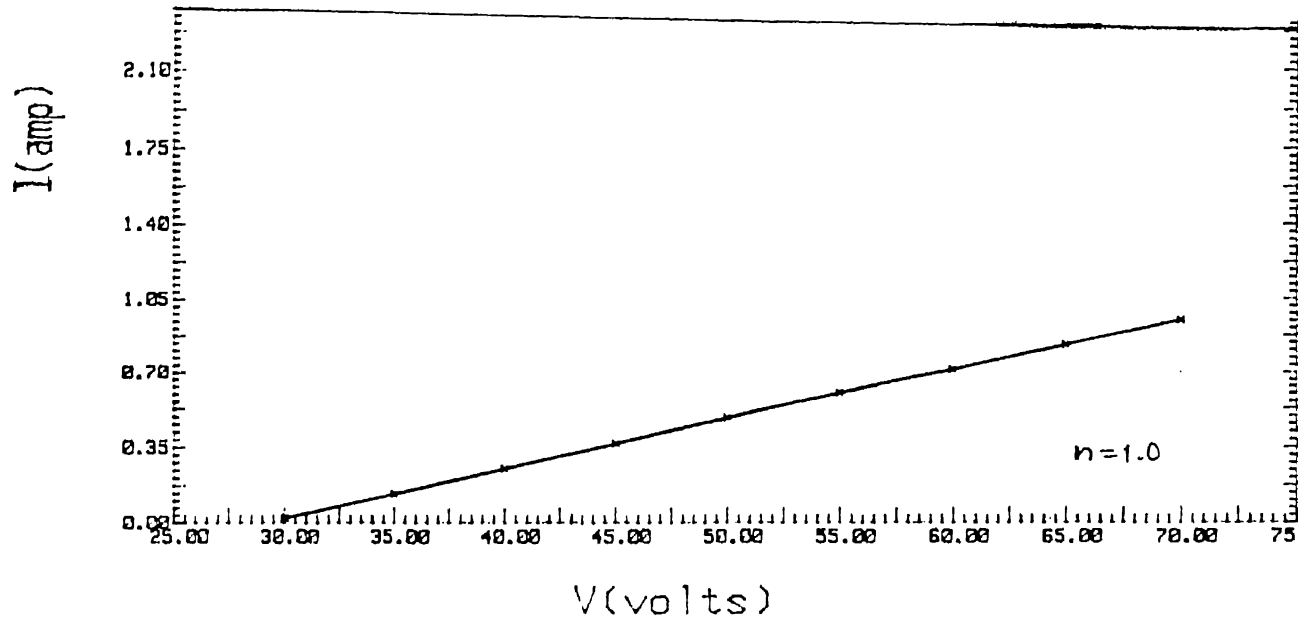

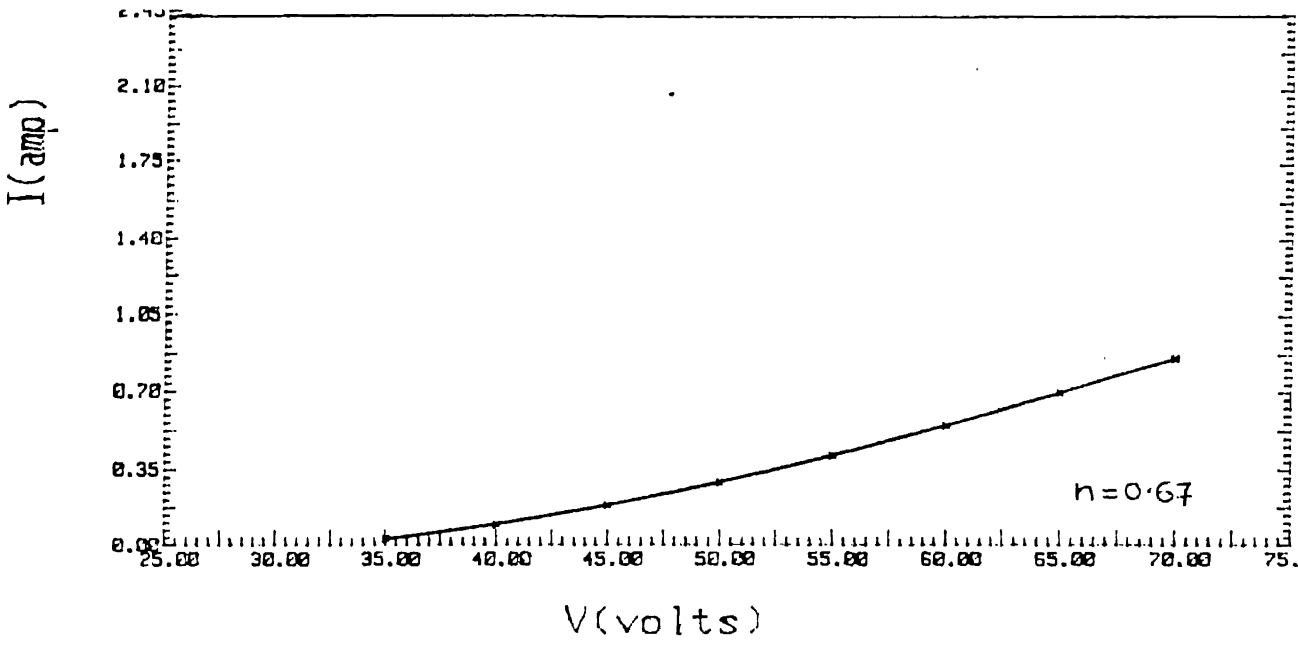

Figure 2.5: V I Characteristics for Arc Valve A=29, B=37

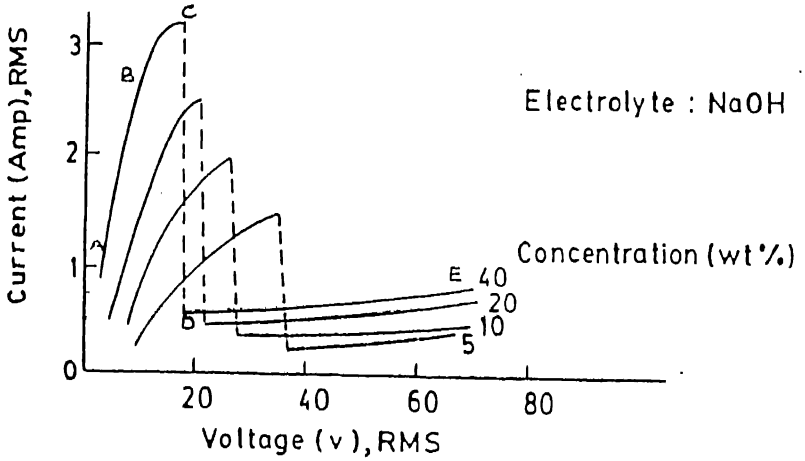

Tool dia = 0.11 cm ; Tool depth = 0.2 cm
Smooth D.C.

V-I Characteristic for different concentration of electrolyte

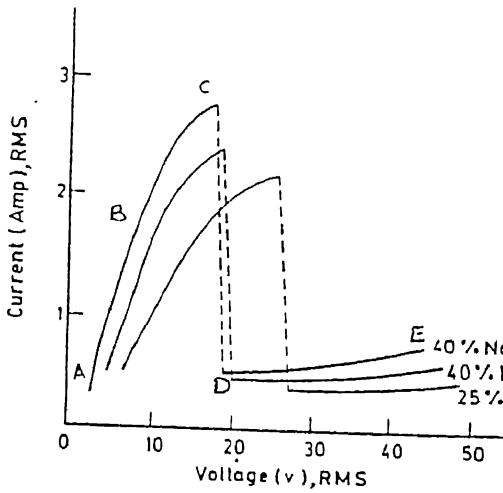

Tool dia : 0.11 cm Tool depth :=0.2 cm
Power supply : Smooth D.C.

V-I Characteristics for different

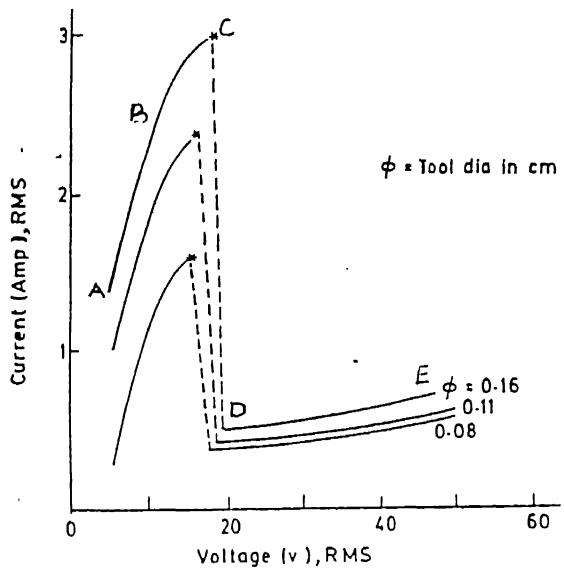

Electrolyte : 40 % KOH ; Power supply : Smooth D.C. ;
Depth in electrolyte : 0.2 cm

V-I Characteristic for different tool diameter

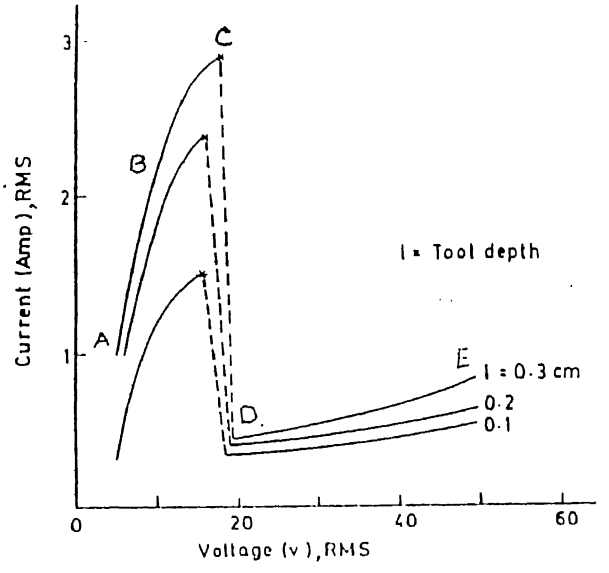

Electrolyte : 40 % KOH ; Tool diameter : 0.11 cm ;
Power supply : Smooth D.C.

V-I Characteristic for different tool dep

Figure 2.6: A typical V I Characteristics of ECSM process

Where

Vs = Supply voltage (volt)

K = Conductivity of electrolyte (mho/m)

ϕ = Diameter of cathode (cm), and

d = Depth of tool inside electrolyte (cm).

Using experimental results of Basak [2], and employing multivariable curve fitting technique, the following equation have been obtained :

$$I = 0.1009 V_s^{0.4815} K^{0.3420} \phi^{0.3936} d^{0.2881} \tag{2.5}$$

where

$$20 < Vs < 70 \qquad volt \tag{2.6}$$

$$30 < K < 50 \qquad mho/m \tag{2.7}$$

$$0.8 < \phi < 1.1 \qquad cm \tag{2.8}$$

$$0.0 < d < 3.0 \qquad cm \tag{2.9}$$

Equation(2.5) gives maximum error of 7.0 percent with respect to the experimental results as shown in Table 2.1.

The values of electrolyte conductivity K (mho/m) can be obtained from the relationship between electrolytic conductivity K (mho/m) and percentage concentration (C) by weight of electrolytes. The following equations have been obtained for electrolytes using the data given in reference [18] :

For NaOH

$$K = 0.885958 + 4.62384C - 0.193274C^2 + 0.00208907C^3 \tag{2.10}$$

for KOH

$$K = -0.335781 + 3.86262C - 0.0680216C^2 \tag{2.11}$$

for NaCl

$$K = -0.0154902 + 1.46172C - 0.0243105C^2 \tag{2.12}$$

at 18 celcius.

The curves for electrolyte conductivity and percentage concentration by weight are given in Appendix A.

v volt	k mho/m	Dia cm	depth cm	I(amp) Th.	I(amp) Exp	% difference (w.r.t. exp)
20.0000	45.3345	.0800	.2000	.3663	.3726	1.6964
30.0000	45.3345	.0800	.2000	.4453	.4314	3.2108
40.0000	45.3345	.0800	.2000	.5114	.5098	.3153
50.0000	45.3345	.0800	.2000	.5694	.6078	6.3148
20.0000	45.3345	.1100	.2000	.4152	.4216	1.5202
30.0000	45.3345	.1100	.2000	.5047	.4706	7.2479
40.0000	45.3345	.1100	.2000	.5797	.5490	5.5917
48.0000	45.3345	.1100	.2000	.6329	.6176	2.4761
50.0000	45.3345	.1100	.2000	.6455	.6569	1.7420
20.0000	45.3345	.1600	.2000	.4812	.5098	5.6164
30.0000	45.3345	.1600	.2000	.5849	.5686	2.8685
36.0000	45.3345	.1600	.2000	.6386	.6274	1.7824
40.0000	45.3345	.1600	.2000	.6718	.6667	.7674
46.0000	45.3345	.1600	.2000	.7186	.7451	3.5585
30.0000	32.8400	.1100	.2000	.4520	.4722	4.2745
40.0000	32.8400	.1100	.2000	.5192	.5000	3.8353
50.0000	32.8400	.1100	.2000	.5781	.5556	4.0441
60.0000	32.8400	.1100	.2000	.6311	.6389	1.2186
70.0000	32.8400	.1100	.2000	.6797	.6944	2.1108
20.0000	45.3345	.1100	.1000	.3400	.3600	5.5448
30.0000	45.3345	.1100	.1000	.4134	.4000	3.3383
40.0000	45.3345	.1100	.1000	.4748	.4600	3.2108
50.0000	45.3345	.1100	.1000	.5286	.5400	2.1065
20.0000	45.3345	.1100	.2000	.4152	.4200	1.1451
26.0000	45.3345	.1100	.2000	.4711	.4600	2.4134
30.0000	45.3345	.1100	.2000	.5047	.5000	.9417
36.0000	45.3345	.1100	.2000	.5510	.5400	2.0410
40.0000	45.3345	.1100	.2000	.5797	.5800	.0520
46.0000	45.3345	.1100	.2000	.6201	.6400	3.1165
30.0000	45.3345	.1100	.3000	.5672	.5400	5.0447
40.0000	45.3345	.1100	.3000	.6515	.6600	1.2844
46.0000	45.3345	.1100	.3000	.6969	.7400	5.8272

Table 2.1: Multivariable Curve Fitting Output

It should be noted at this point that, the resistance of the electrolyte changes during the process due to increased percentage of dissolved graphite and machined workpiece material and vaporization of electrolyte. The change in resistance of bulk electrolyte greatly affects the cell current but the technique used incorporates all theses effects as the data has been taken from the experimental results.

2.6 Determination of Hydrogen Bubble Diameter

The intensity of the electric field (E) required to produce a spark in an arc discharge valve is of the order of 10^6 volt per meter. If the resistance of the bulk electrolyte is R_i and circuit current is I then the voltage drop in the H_2 bubble which is equivalent to an arc discharge valve (Figure2.4d) is given by

$$V_b = V_s - R_i I. \tag{2.13}$$

Here the voltage drop due to inherent circuit elements is neglected.

Therefore the approximate diameter of the H_2 bubble which is analogous to the distance between two parallel electrodes is

$$d_b = \frac{V_b}{E} \tag{2.14}$$

where E is the intensity of Electric Field required to produce the spark.

The current ranges from 0.1 to 1.2 ampere in case of electrochemical spark machining and supply voltage (V_s) is kept in between 30 to 60 volts. The resistance of bulk electrolyte is generally less than 10 ohms . Thus taking V_b ranging from 25 to 55 volts the bubble diameter range would lie between 25 microns to 55 microns. However, due to memory and computational limitations, the bubble diameter has been taken as constant and equal to 200 micrometer.

2.7 Explanation of V I Characteristics of the ECSM process using Valve Theory

Figure 2.6 shows a typical V I characteristics of the ECSM process. The curve can be divided into four regions -

AB - Straight variation,

BC - Curved variation,

CD - Transition, and

DE - Sparking.

For the region AB and BC the equivalent circuit for the process is shown in Figure 2.4.a. In the region AB the current varies in proportion to the voltage and hence Ohm's law holds good. From B to C the bubble density on the cathode increases which offers extra resistance in the path of current and hence the rate of increase of current decreases. Point C is a critical point at which the whole tool inside the electrolyte is accumulated with bubbles and sparking starts. In the region AB and BC the current is higher than the sparking region and the power drawn from the DC source is spent in Joul's $(V_s^2/(Ri + R^*))$ heating of the electrolyte solution.

At point C, when the whole tool is covered with the bubbles and the current can pass only through the common region of the two bubbles (bubble bridge), it offers a high resistance to the current so there is a drastic decrease in the circuit current. At this stage the energy supplied by the DC source is spent in heating of the electrolyte as well as in sparking which gives productive energy. Therefore a transition is observed from C to D.

Region DE is a sparking region where the current is a function of number of parameters like supply voltage, electrolyte conductivity, diameter of tool and depth of tool inside the electrolyte [**2**].

Chapter 3

Theoretical Formulation and FEM Implementation

The process of material removal in ECSM process consists of thermal melting or softening in the case of amorphous materials and/or vaporization. A part of the energy released by a spark is conducted into the workpiece and raises its temperature to a high value. This temperature rise is confined to a localized region if the thermal conductivity of the workpiece material is poor. When the maximum temperature attained exceeds the melting (or softening) temperature of the workpiece, that part of the workpiece melts or softens and may vaporize also. The molten part of the workpiece is assumed to be removed by the shock waves resulting due to the extinction of sparks. However, in real life, some part of the molten material is not removed because of quenching effect by surrounding electrolyte. Due to quenching effect, the molten or softened material resolidifies and adheres to the parent material. As a result of this, the ejection efficiency comes into the picture. This plays very dominant part as the ejection efficiency in ECSM, is very low. It may be as low as about 10 percent or even lower than that. The volume of the material removed during each spark can be calculated from the volume of the crater formed.

3.1 Theoretical formulation

Since the real life problems are three dimensional in nature, the problem is formulated as a 3-D unsteady state heat conduction problem with Neumann and **Robbins** boundary

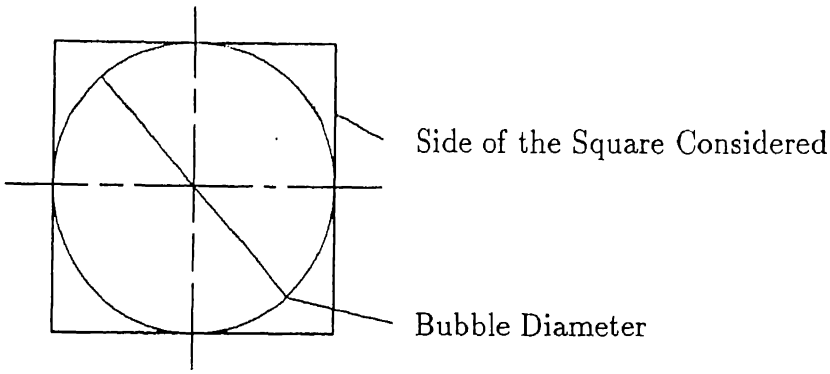

Figure 3.1: Heat source Idealization

conditions. Location of heat source is assumed to vary randomly with the time. The heat source (spark) is modeled as uniformly distributed heat source however some authors [26,27] have taken Gaussian heat source for the analysis of EDM but for the simplification of the analysis, uniformly distributed cylindrical heat source is assumed in the present analysis. The heat source (spark) is usually cylindrical in nature but in order to facilitate computation it has been considered as a prismatic channel with square cross section and its cross sectional area is taken to be approximately equal to the area of cross section of cylindrical channel (refer Figure 3.1). The spark acts on the workpiece surface for a certain period of time (t_d) and then disappears. Immediately after this another heat source starts acting but at a different location (governed by a random number as explained later) on the workpiece and the process is repeated. With every spark some material is removed by melting and/or by vaporization or by softening in the case of amorphous materials.

3.1.1 Assumptions

The following assumptions and idealization are proposed to simplify the model of material removal in ECSM.

1. The workpiece is homogeneous and anisotropic.

2. During discharging the current flow through the other part of the electrode (cathode) surface is negligible.

3. All sparks are identical.

4. A spark is considered as uniformly distributed heat source over a square area .
5. The duration (t_d) of sparking is same for all the sparks.
6. No time gap between any two consecutive sparks is considered (ie off time is taken as zero).
7. The energy density of a spark column is constant.
8. The total molten part of the workpiece is assumed to be removed from the machining zone (ie 100 percent ejection efficiency is assumed).
9. Thermal efficiency is also assumed to be 100 percent (ie the total heat generated due to spark goes into the workpiece. However, a part of it is convected to the electrolyte from the exposed surface of the workpiece).
10. Radiation losses to the atmosphere are assumed to be zero.
11. Heat conducted to the electrolyte is also assumed to be zero.

3.1.2 Governing Differential Equation

The temperature T at any point of the workpiece due to the action of heat source is given by the **Heat diffusion equation**

$$\rho C_p \frac{\partial T}{\partial t} = \frac{\partial}{\partial x_i}[K_{ij}(\frac{\partial T}{\partial x_j})] \tag{3.1}$$

where,

ρ = Density of the workpiece material

C_p = Specific heat of the workpiece material

t = time

K_{ij} = Thermal conductivity

x_i,x_j = Space coordinates where i and j vary from 1 to 3.

Thermal conductivity and specific heat are the functions of temperature. Thermal Conductivities K_x,K_y and K_z will be useful for analysis of a composite drilling with ECSM, by considering the equivalent homogeneous, anisotropic material.

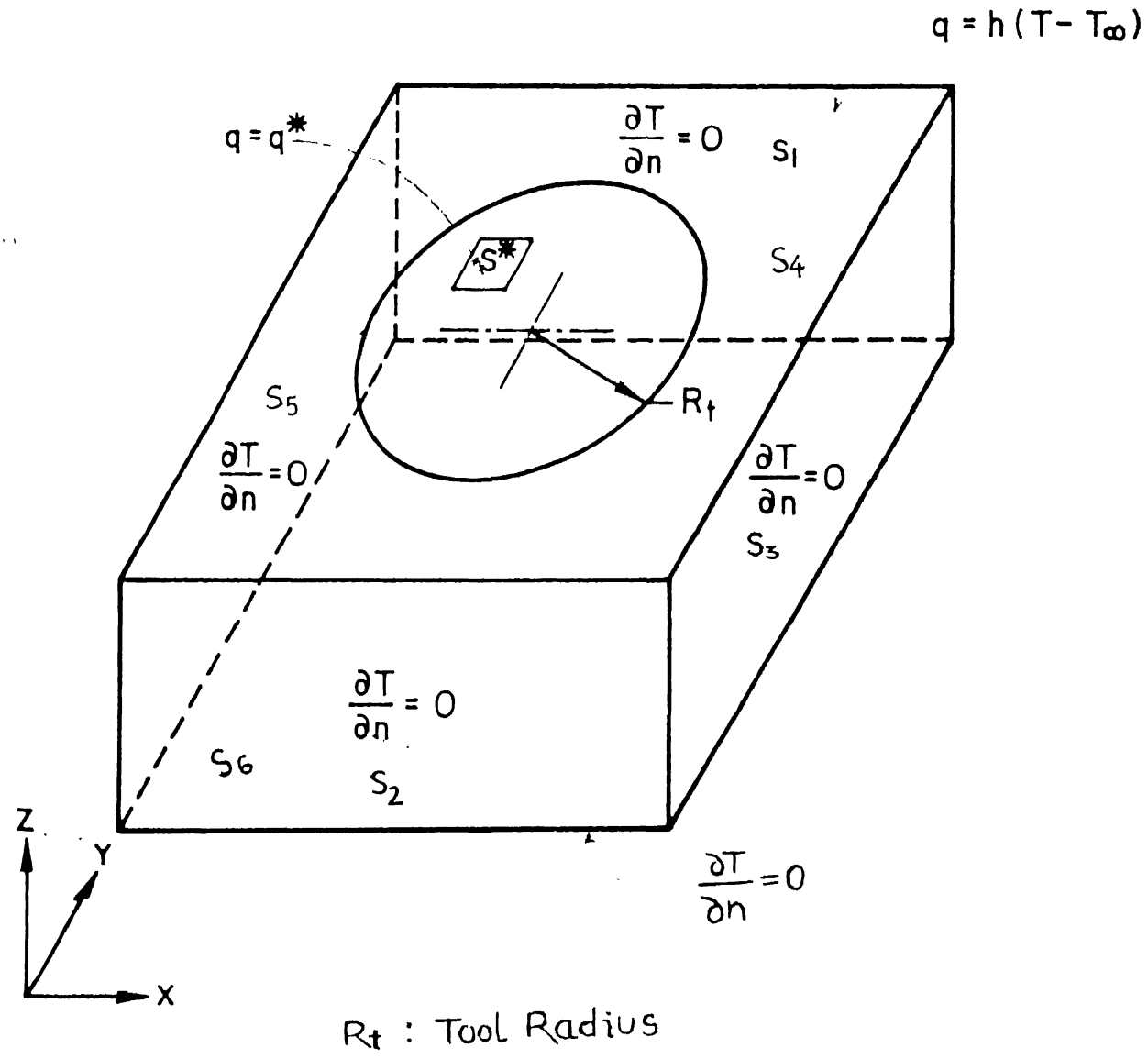

Figure 3.2: Workpiece domain considered for Finite Element analysis

3.1.3 Boundary Conditions and Initial Condition

The cubical part of a workpiece below the tool is considered as a domain for the analysis such that the flow of heat across the planes (refer Figure 3.2) S_2, S_3, S_4, S_5, S_6 is negligible ie

$$\frac{\partial T}{\partial n} = 0 \qquad on \ S_2, S_3, S_4, S_5, S_6 \qquad for \ t \geq 0 \tag{3.2}$$

On the top surface of the workpiece, area S^* receives heat and its location varies with the time t. q^* is the heat received by the area S^* for a time period t_d after that no heat is received by this area, and another spark is produced at some other location governed by the random number generation.

$$so, \qquad q = q^*, \qquad on \ S^* \qquad t \leq td \tag{3.3}$$

$$q = 0 \qquad t > td \tag{3.4}$$

Where q^* is spark energy density (refer section 2.5).

The surface area on the top of the workpiece S_1 looses heat due to convection to the surrounding electrolyte therefore,

$$q = h(T - T_\infty), \qquad on \ S_1 \qquad for \ t \geq 0 \tag{3.5}$$

where

h=Convective heat transfer coefficient

T_∞ =Ambient temperature of electrolyte

q = Heat transfer rate.

The initial condition for the problem is that at time t is equal to zero, the whole workpiece remains at its initial temperature ie

$$T(x, y, z, 0) = T_{unif} \tag{3.6}$$

where T_{unif} is initial temperature of workpiece.

3.2 Solution procedure by Galerkin FEM

The problem has been formulated for temperature evaluation at a point in a 3 D workpiece,in the previous section. The domain for the problem is three dimensional. The material properties change with the temperature and their variations are complicated. The problem is unsteady and location of the heat source changes with time which makes the problem more complicated. The Finite Element Method (FEM) suits ideally for solving such a problem. 3 D problems with variation in material properties and heat sources can be handled with ease in this approach. It also facilitates implementation of the convective boundary conditions. Therefore, Galerkin's method of weighted residuals has been employed in this work.

The residual expression for the above problem is given by the following equation:

$$\int_v [K_x \frac{\partial w}{\partial x}\frac{\partial T}{\partial x} + K_y \frac{\partial w}{\partial y}\frac{\partial T}{\partial y} + K_z \frac{\partial w}{\partial z}\frac{\partial T}{\partial z}]dV + \int_v \rho C_p \frac{\partial T}{\partial t} w dV + \int_{s_1} h(T - T_\infty) w ds$$

$$+ \int_{s^*} q^* w ds = 0 \tag{3.7}$$

where w is weighted function, V and v stand for volumes, S and s stand for surfaces.

The cubical domain considered for the analysis has been discretized into eight noded brick element with one degree of freedom (temperature) per node. The element used is shown in Figure 3.3. Approximation for temperature is assumed as

$$T = N^{eT} T^e = T^{eT} N^e \tag{3.8}$$

where N^e = shape function matrix.

W^e = Matrix corresponding to the weight function

Then for Galerkin FEM

$$w = N^{eT} W^e = W^{eT} N^e \tag{3.9}$$

Using equations (3.8) and (3.9), equation (3.7) can be rewritten as

$$[GC]\frac{\partial T}{\partial t} + [GK]T = Q \tag{3.10}$$

[GC] and [GK] in the above equation are global specific heat and global thermal conductivity matrices. Q is the right side vector. These matrices are expressed by the following expressions:

$$[GC] = \sum_{e=1}^{ne} [A]^{eT} [C]^e [A]^e \tag{3.11}$$

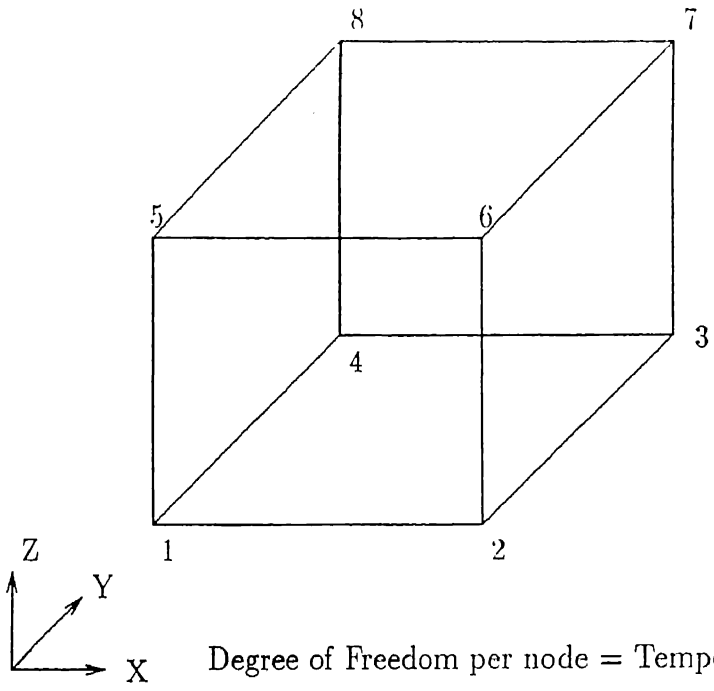

Figure 3.3: 3-D Brick Element

$$and \qquad [C]^e = \int_v \rho C_p N^e N^{eT} dv \tag{3.12}$$

where $[C]^e$ is elemental specific heat matrix and ne is number of volume elements.

Global conductivity matrix is given by

$$[GK] = \sum_{e=1}^{ne} [A]^{eT} [K\prime]^e [A]^e + \sum_{s=1}^{ns_1} [S_1]^{sT} [H]^s [S_1]^s \tag{3.13}$$

(Matrices [A] ans [S] are described later)

where

$$[K\prime]^e = \int_v [K_x N_x{}^e N_x{}^{eT} + K_y N_y{}^e N_y{}^{eT} + K_z N_z{}^e N_z{}^{eT}] dv \tag{3.14}$$

and

$$[H]^s = \int_{s_1} h N^{sT} N^s ds, \tag{3.15}$$

$[K]^e$ = Elemental conductivity matrix,

$[H]^s$ = Surface elemental convective heat loss matrix, and

ns_1 = Number of surface element on surface S_1.

Right hand side vector Q in equation (3.10) is difference of two matrices

$$Q = Q_2 - Q1 \tag{3.16}$$

Where the expressions for Q_2 and Q_1 are:

$$Q_2 = \sum_{s=1}^{ns_1} Q_2^s [S_1]^s \tag{3.17}$$

$$Q_1 = \sum_{s=1}^{ns^*} Q_1^s [S^*]^s \tag{3.18}$$

and

$$Q_2^s = \int_{s_1} hT_\infty N^s ds \tag{3.19}$$

$$Q_1^s = \int_{s^*} q^* N^s ds \tag{3.20}$$

Where

N^e = Shape function for the volume elements

N^s = Shape functions for the surface elements

A_{ij} and S_{ij} are the matrices such that

$$A_{ij} = \delta_{ij} \qquad j = C(e,i) \tag{3.21}$$

$$S_{ij} = \delta_{ij} \qquad j = S(s,i) \tag{3.22}$$

where δ = Kronecker delta.

C and S are volume element and surface element connectivity matrices respectively. Superscripts s is for surface elements and e is for volume elements.

Implicit Finite Difference scheme is used to convert set of linear differential equations (3.10) to simultaneous algebraic equations (3.23).

$$[A]_{i+1} T_{i+1} = F_{i,i+1} \tag{3.23}$$

where i is suffix for time steps and

$$[A]_{i+1} = \frac{[C]}{(\delta t)_{i+1}} + [K] \tag{3.24}$$

$$F_{i,i+1} = Q_{i+1} + [B]_{i+1} T_i \tag{3.25}$$

In the above equation $[B]_{i+1}$ is given by

$$[B]_{i+1} = \frac{[C]}{(\delta t)_{i+1}} \tag{3.26}$$

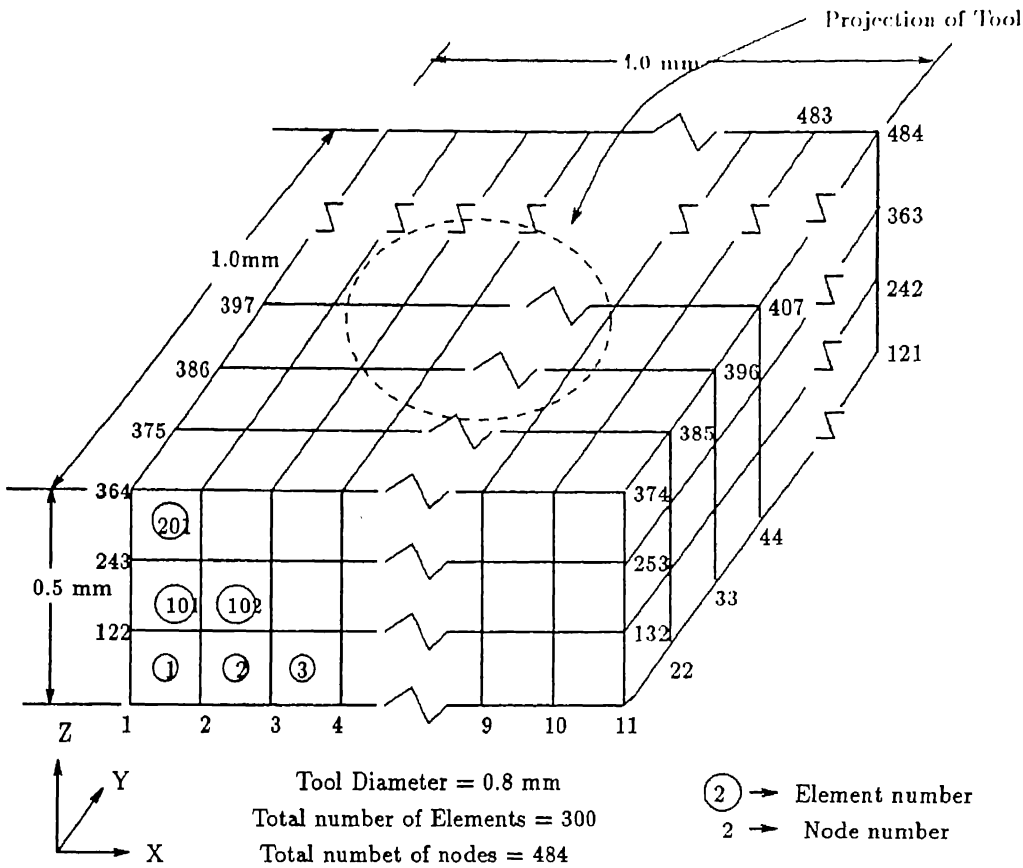

Figure 3.4: Node numbering scheme

where [C] global specific heat matrix, Q is right side vector and δt is the time step for temperature computation.

Simultaneous algebraic equations (3.23) are solved by the Householder method in order to get the temperature distribution.

3.3 Features of the Finite Element Code

3.3.1 Mesh generation

The code has an automatic mesh generation routine which takes the size of the domain and number of divisions in X, Y and Z directions as input parameters. It computes the nodal coordinates and connectivity matrix. This routine also generates surface connectivity matrix for four noded two dimensional surface elements, which are utilized for convection boundary conditions and heat supply conditions.

The node numbering and element numbering schemes used are shown in Figure 3.4

3.3.2 Temperature dependent workpiece properties

Heat conduction equation involves thermal conductivity and specific heat of the material as important thermal properties. These properties are very much dependent on the temperature.

The problem is unsteady heat conduction therefore after a each time step these properties have been altered according to latest temperature. The details of the same are given in Appendix B.

3.3.3 Random location of heat source

During actual ECSM process, the physical laws which govern the location of spark on the tool (or in the vicinity of the workpiece) are not known. It is also not known whether multiple sparks, or single spark is produced at a time. Further, the spark generated is on the bottom face of the tool, or the side surface of the tool, is also not known. With such a fuzziness in the system, it is extremely difficult to accurately model the location of a spark during the process, and that too without having the knowledge of the laws of the the nature governing them.

With the above facts in view, the location of a spark is assumed to be governed by the random numbers generated using the standard Nag routine. For this purpose, each node on top surface of the workpiece is assigned a definite node number for identifying the location of the next sparks. It is also assumed that only one heat source acts at a time on the workpiece, and after discharge time t_d, another spark is generated at another location. A condition is also imposed that this number generated by Nag routine should be within the number lying in a circle on the top surface of the workpiece, and circle is the projection of a circular cross sectioned tool on the workpiece.

A single node number is obtained randomly, and all four surface elements (s_1, s_2, s_3 and s_4 of Figure 3.5) which are belonging to it are chosen as s^* that is the area for which heat is supplied.

3.3.4 Circuit current and heat flow rate

The code computes the circuit current by different input parameters like voltage, concentration of the particular electrolyte (NaoH, KOH or NaCl), diameter of cathode and cathode

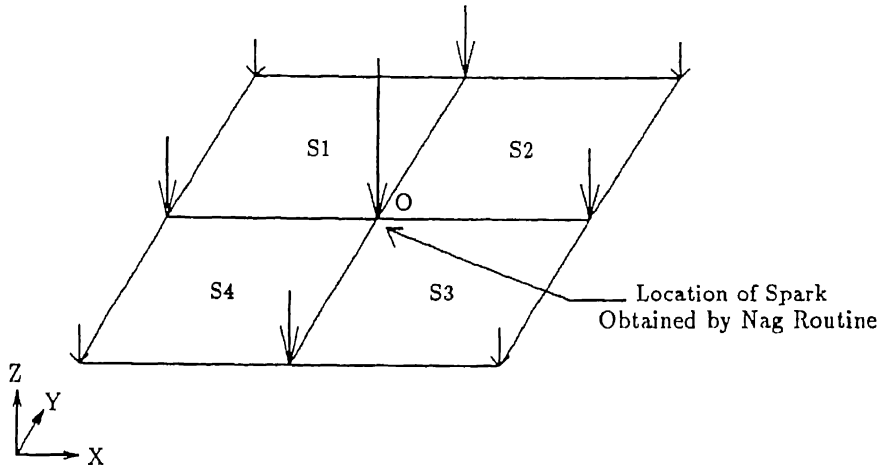

Figure 3.5: Four noded surface element

depth inside electrolyte, using equation (2.5). The resistance of bulk electrolyte is supplied as an input parameter which is equivalent to the slope of straight portion (ie no sparking) of V I curve (Figure 2.6) of the process for particular operating conditions.

Using the appropriate relation (equation 2.1) it calculates heat flow rate for sparks (refer section 2.4).

3.3.5 Consideration of material removed by previous spark

During each spark, that amount of material is assumed to be removed which attains temperature equal to or above melting / softening temperature. However, it is very difficult to consider the exact domain for computation because of irregular shapes of the crater. Therefore, in this work a simplified approach is used. The conductivity and specific heat are assigned the value zero for further calculations when the temperature of a particular node exceeds or equals softening temperature of the workpiece material. In this way contribution of these nodes to the conductivity and specific heat matrix during subsequent calculations are made zero. As a result, it does not require to modify the discretization after every spark.

3.3.6 Material removed per spark

Material removed per spark is computed by multiplying the volume of the softened material by its density. The volume of the crater is computed by interpolating the temperature on the

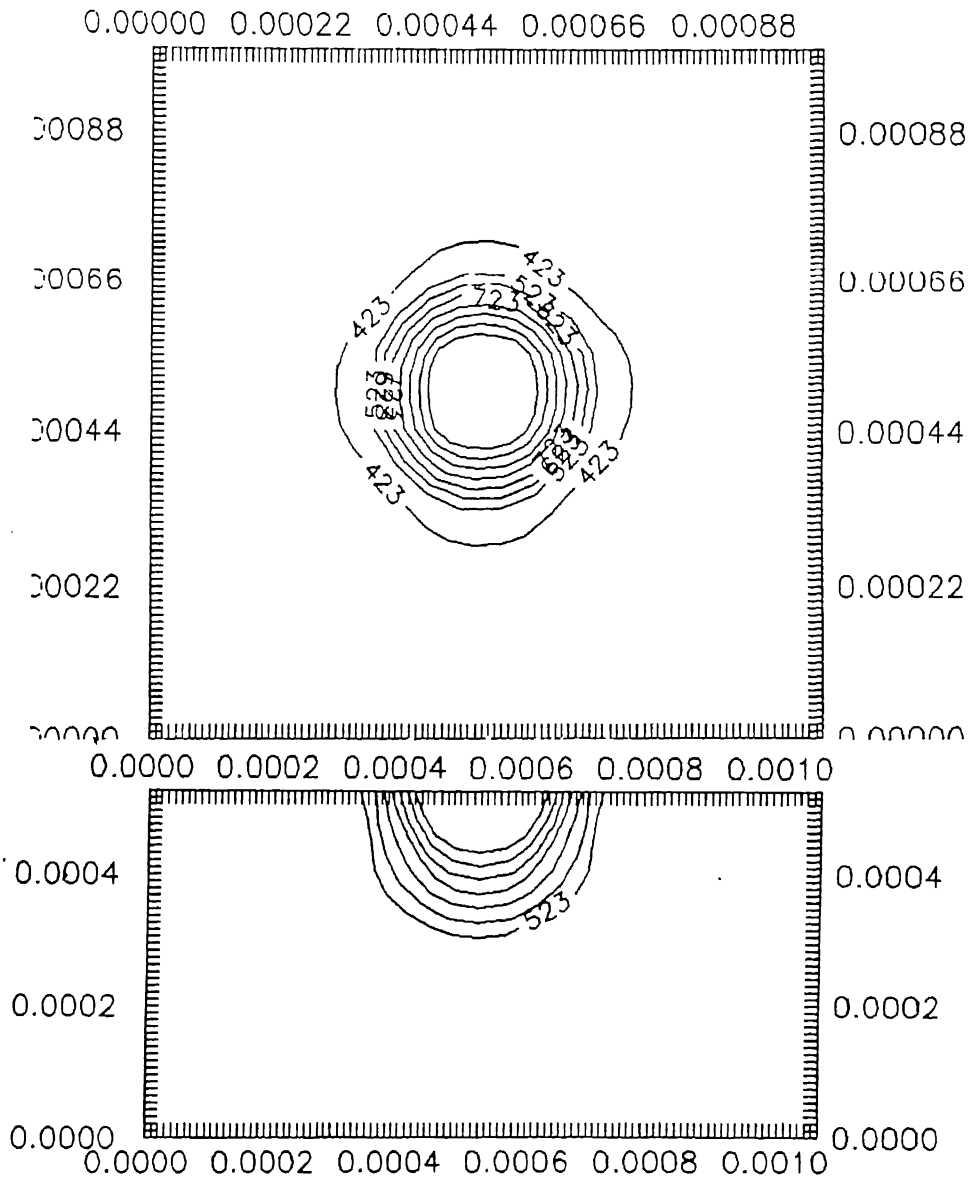

Figure 3.6: Isotherms for single spark

top surface for softening temperature and similarly in the depth. By single spark isotherm plots obtained on top and depth as shown in Figure 3.6 , it has been concluded that the crater can be well approximated by an hemi ellipsoid. Volume V of the hemi ellipsoid is given by the following equation :

$$V = \frac{2}{3}\pi abc \tag{3.27}$$

where a,b and c are the half of the axes of the ellipsoid.

3.4 Flowchart

The flowchart for the developed computer code is given on the next page. (Figure 3.7)

3.5 Closure

The program for the implementation of FEM has been developed in Fortran 77. It was run on HP super mini computer (Agni, CPU time for each run is 17.5 minutes), for different input parameters to test the validity of the formulation. The results and discussions are described in the following chapter.

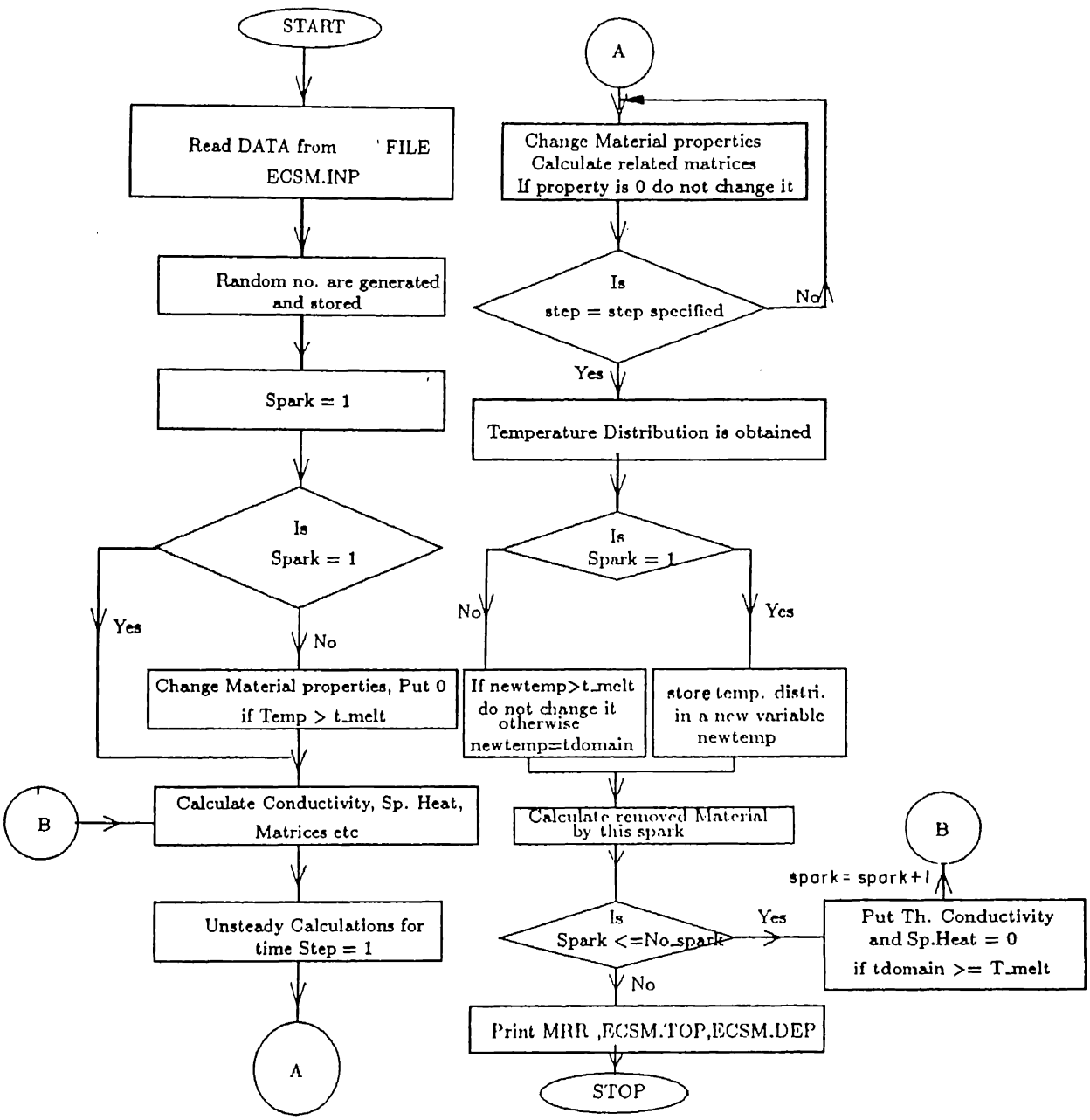
START
Read DATA from FILE ECSM.INP
Random no. are generated and stored
Spark = 1
Is Spark = 1
Yes
No
Change Material properties, Put 0 if Temp > t_melt
B
Calculate Conductivity, Sp. Heat, Matrices etc
Unsteady Calculations for time Step = 1
A
A
Change Material properties Calculate related matrices If property is 0 do not change it
Is step = step specified
No
Yes
Temperature Distribution is obtained
Is Spark = 1
No
Yes
If newtemp>t_melt do not change it otherwise newtemp=tdomain
store temp. distri. in a new variable newtemp
Calculate removed Material by this spark
B
spark = spark+1
Is Spark <=No_spark
Yes
Put Th. Conductivity and Sp.Heat = 0 if tdomain >= T_melt
No
Print MRR ,ECSM.TOP,ECSM.DEP
STOP

Chapter 4

Results and Discussion

The finite element formulation for the material removal rate in ECSM process developed in the previous chapter has been applied to different machining conditions. The variations in material removal rate with the supply voltage has been predicted and compared with the available experimental findings. The nature of isotherms in the workpiece domain has also been presented and analyzed for the evaluation of overcut.

The computed results are compared with the experimental data reported by Basak[2] and Gautam[7]. Available literature does not give any information about thermal efficiency and ejection efficiency during ECSM process. In the present work, the overall efficiency of the process is assumed as approximately 0.5 percent. Basak[2] has performed his experiments for the case of Soda Lime glass and Gautam[7] used Borosilicate glass in his experiments. The thermal properties of both glasses and their variation with the temperature have been given in Appendix B.

4.1 Estimation of Overcut by Isotherm plots

The isotherm plots for Soda Lime glass and Borosilicate glass have been shown in Figure 4.1 to Figure 4.5. The different cutting conditions for the purpose of computation are :

Electrolyte : NaOH

Concentration : 35 percent (for Soda Lime glass), 20 percent (for Borosilicate glass)

Tool Diameter : 0.8 mm

Depth of tool inside electrolyte : 2 mm

Workpiece : Soda Lime glass, Borosilicate glass

Softening Temperature of Soda Lime Glass[2] : 1123 K

Softening Temperature of Borosilicate Glass[7] : 1093 K

Gautam[7] has performed experiments with 1.6 mm diameter tool. But in the present computational work, a lower value of 0.8 mm has been used. This has been done to reduce the size of the numerical problem to a level permitted by IIT Kanpur computational facilities.

The softening isotherms for different machining conditions are shown in Figure 4.1 to Figure 4.5. These softening isotherms indicate the shape of the machined hole and the depth wise profile of the generated surface, after time 0.0125 sec.

The shape of the softening isotherms is irregular because, the spark channel has been considered as square in shape. The model would have shown a better profile of machined hole, if the cylindrical spark channel had been considered. But consideration of cylindrical spark channel makes the computation of the nodal coordinates extremely difficult and the incorporation of randomness almost impossible.

The overcuts for the different voltages have been calculated by subtracting the tool radius from the maximum radius of the profile of the drilled hole (Figure 4.6). The average overcut can be calculated by subtracting the tool radius from the average radius of the machined hole. But due to simplicity of the first method, it has been used. It is observed that the calculated overcut increases with the supply voltage(Figure 4.7). It is observed experimentally also [11].

It has been reported [2] that if the voltage is increased sufficiently high the machined depth does not increase proportionally, even though the overcut on the top surface increases appreciably. The computational results (Figure 4.7 and Figure 4.9) also indicate it. This can be explained as follows.

The Top portion of the workpiece receives the heat earlier than the material at lower levels. Thus the increase in the thermal conductivity at the top is more in comparison to its value at the lower levels. As the supply voltage increases, the spark energy increases which causes the increased rate of heating at the top. This increases the thermal conductivity at the top resulting in a larger overcut. Another reason for this is the side sparking of the tool.

Figure 4.8 shows the machined depth obtained by Gautam[7] by scanning the machined specimens with the Electron Microscope. The isotherm plots for the depth shows that the

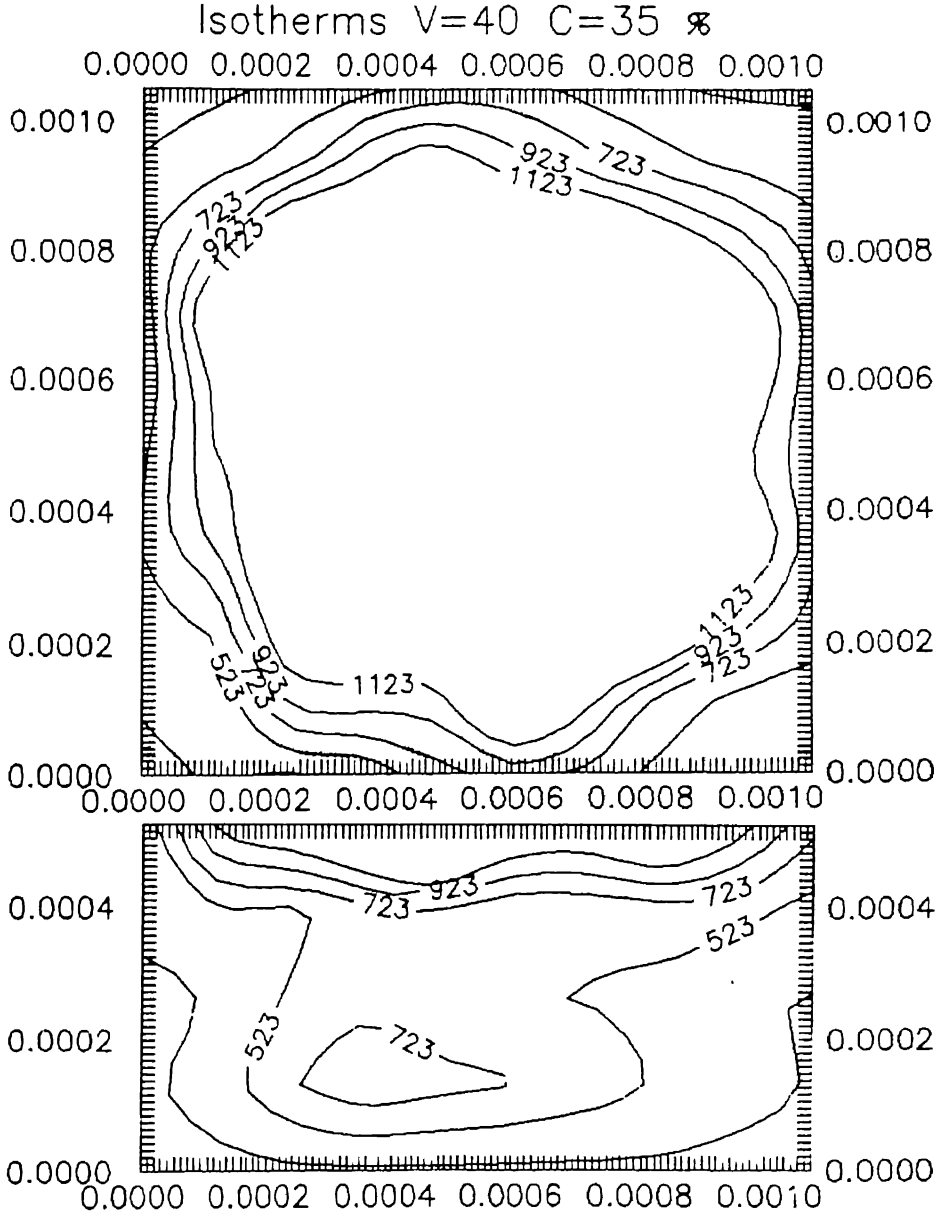

Figure 4.1: Isotherm for V=40, Soda Lime glass

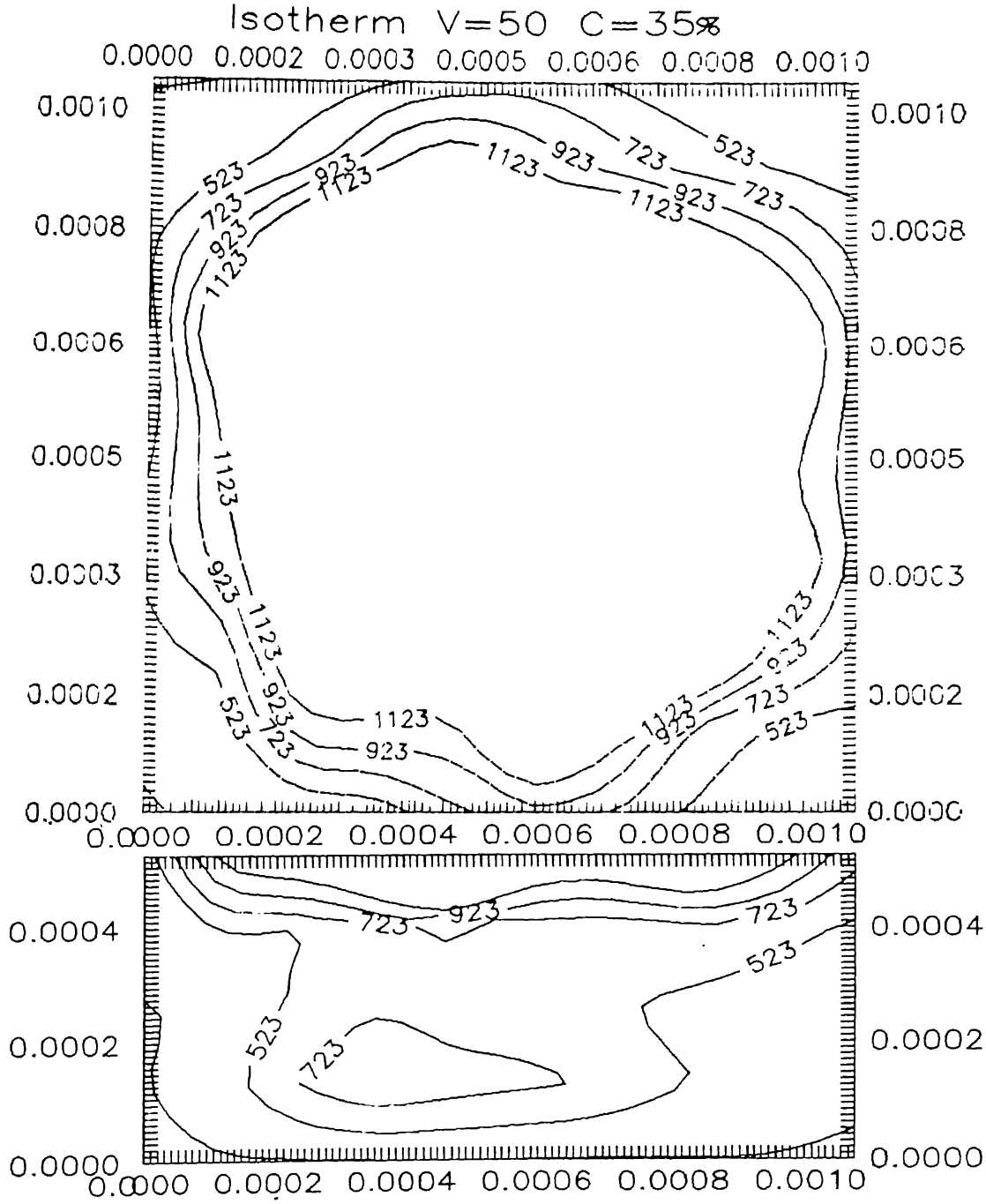

Figure 4.2: Isotherm for V=50, Soda Lime glass

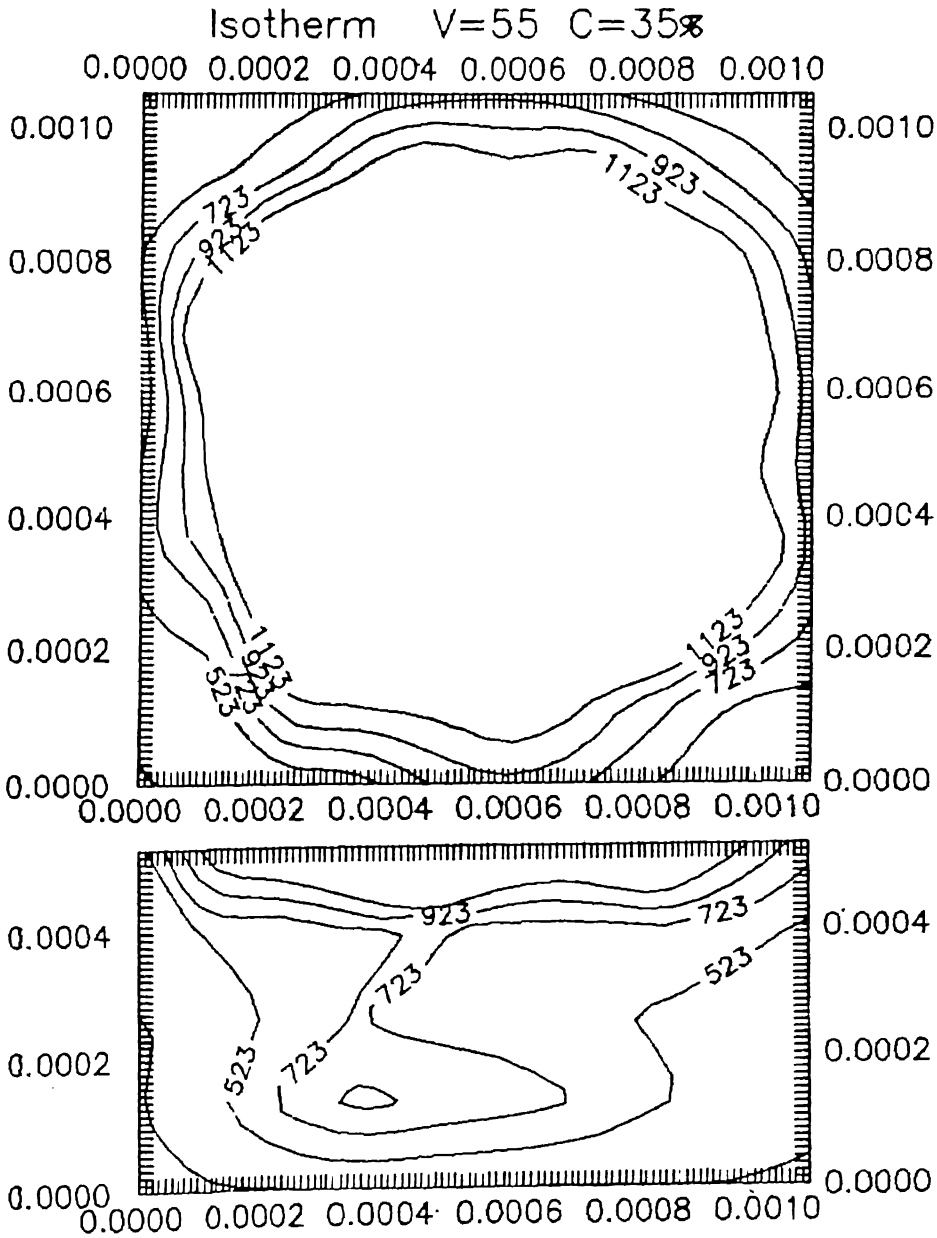

Figure 4.3: Isotherm for V=55, Soda Lime glass

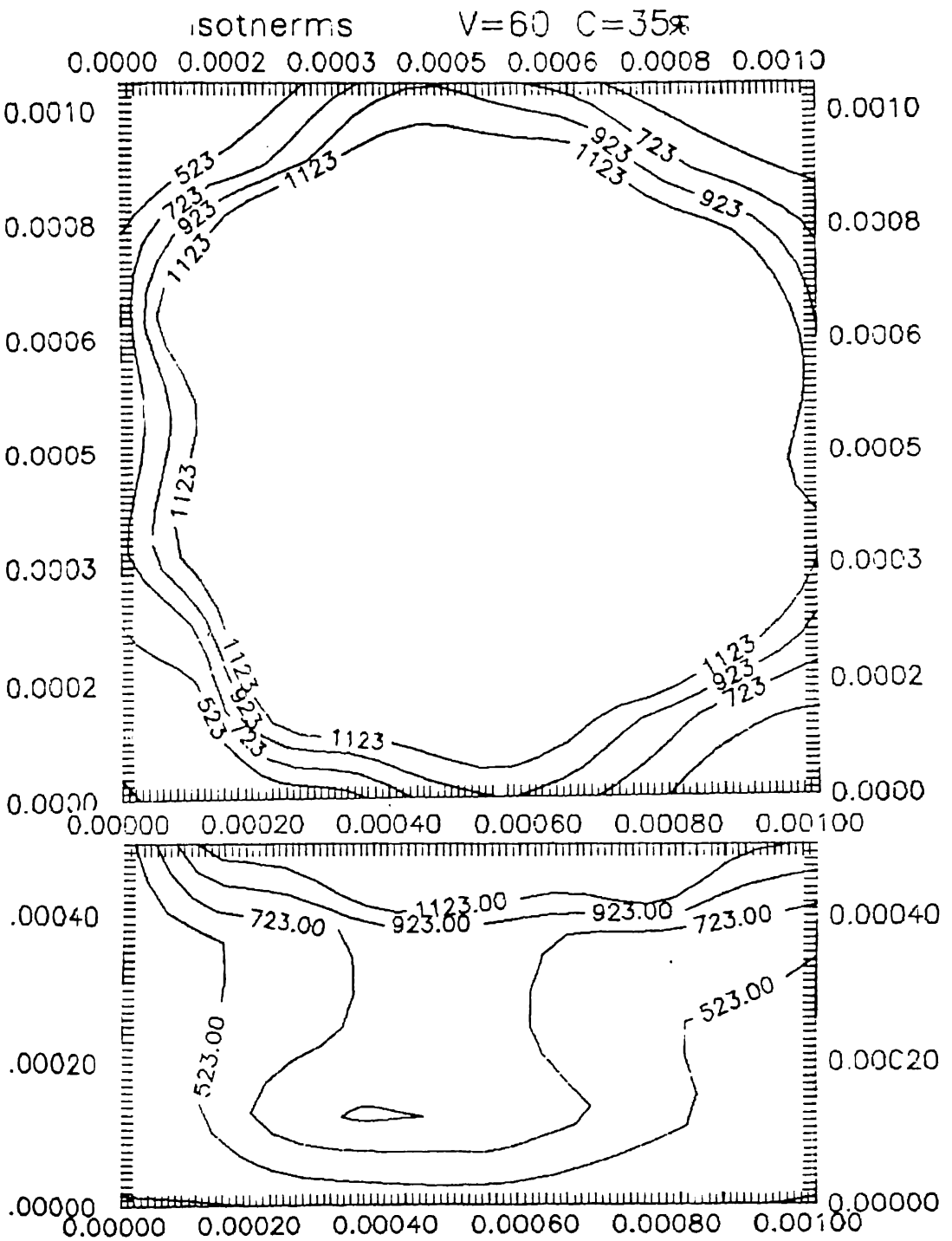

Figure 4.4: Isotherm for V=60, Soda Lime glass

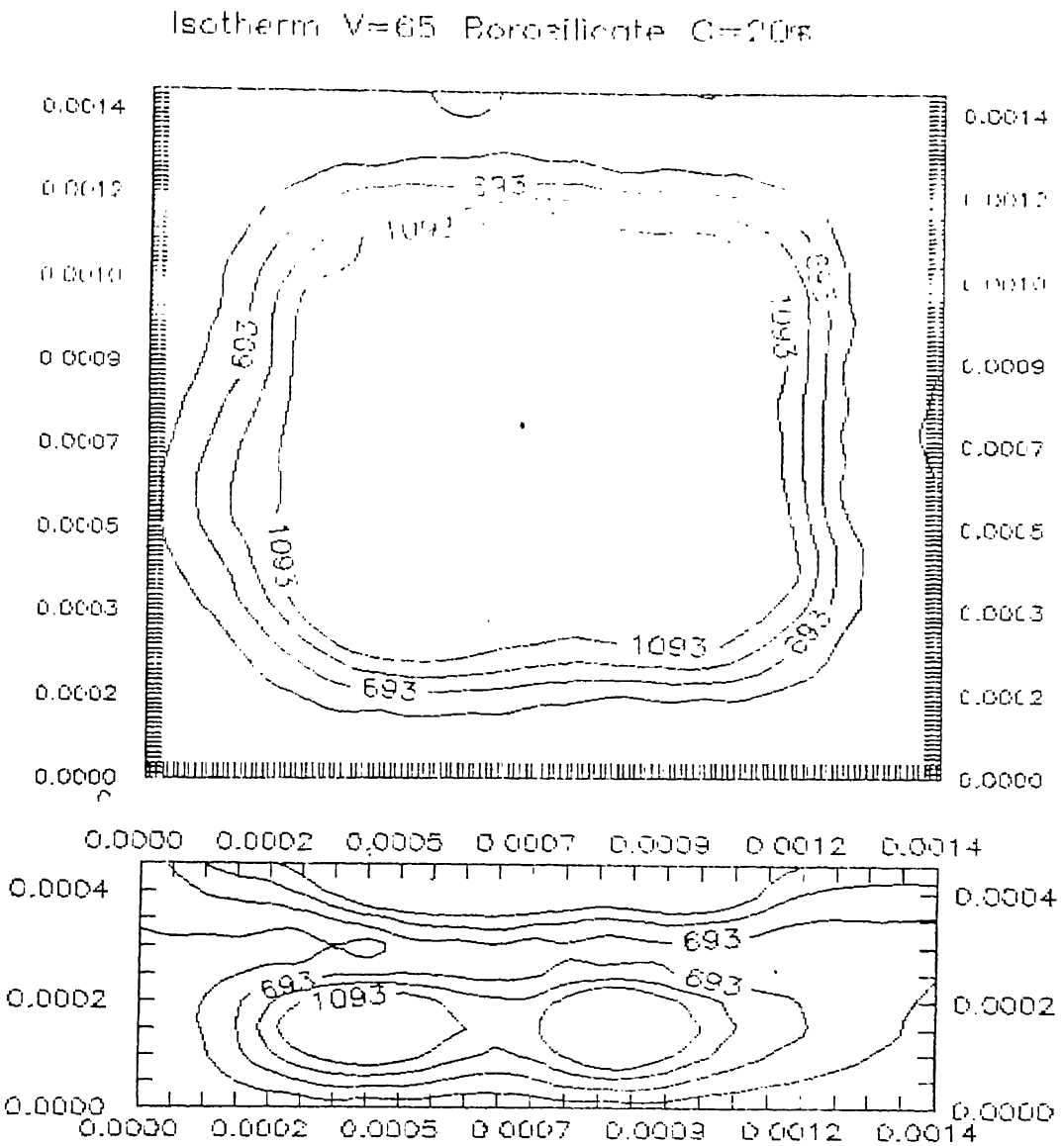

Figure 4.5: Isotherm for V=65, Borosilicate glass

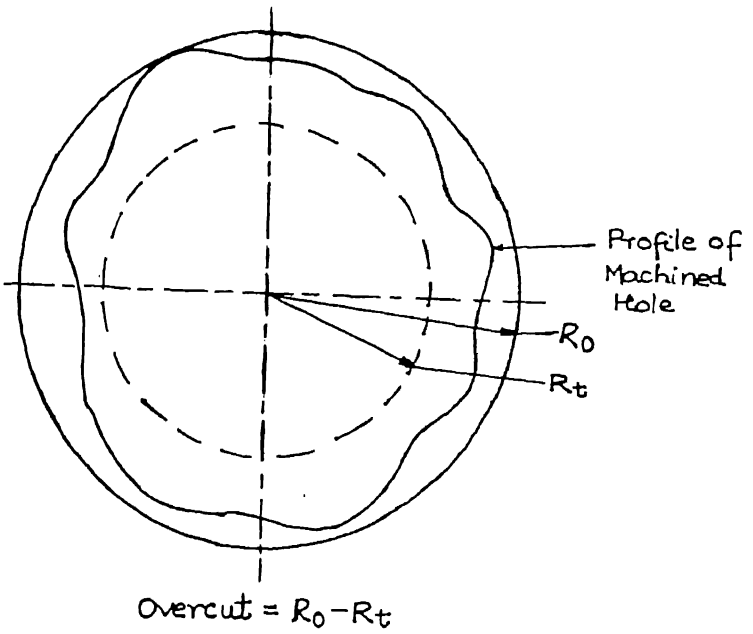

Figure 4.6: Estimation of overcut

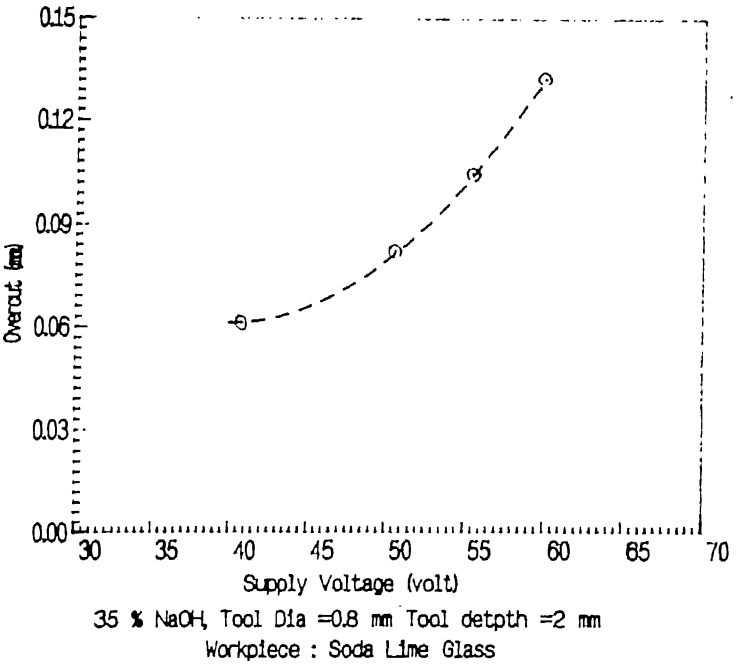

Figure 4.7: Variation of Overcut With Supply Voltage

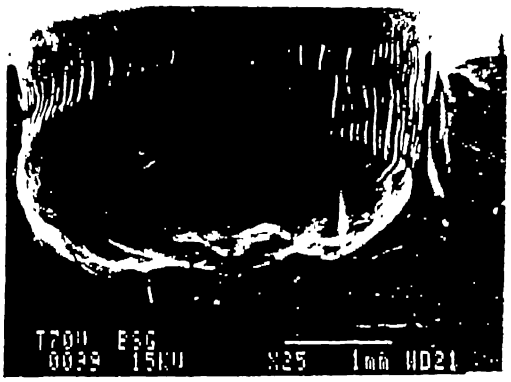

Figure 4.8: Machined Profile by Electron Microscope, 65 volts, Borosilicate glass

type of surface produced experimentally matches with the surface obtained computationally.

Figure 4.9 shows the variation of the maximum penetration of tool with the supply voltage. Figure shows that the maximum penetration depth increases with the increase in supply voltage. Similar thing is observed experimentally (Figure 4.10).

4.2 Material Removal Rate

The Variation of material removal rate with the supply voltage has been plotted in Figure 4.11. The experimental values of material removal rate reported by Basak [2] have also been shown in the same figure. Gautam [7] performed experiments for 65 volt only because his aim was to enhance process capabilities (mainly limited depth characteristics) using various tool arrangements. Computed MRR for 65 volt, 20 percent NaOH concentration, 2.0 mm tool depth inside electrolyte and 0.8 mm tool diameter has been given in Table 4.1

For all cases, the computed material removal rate is observed to be larger than the experimental values, although the trend of variation is same. This is because of the following

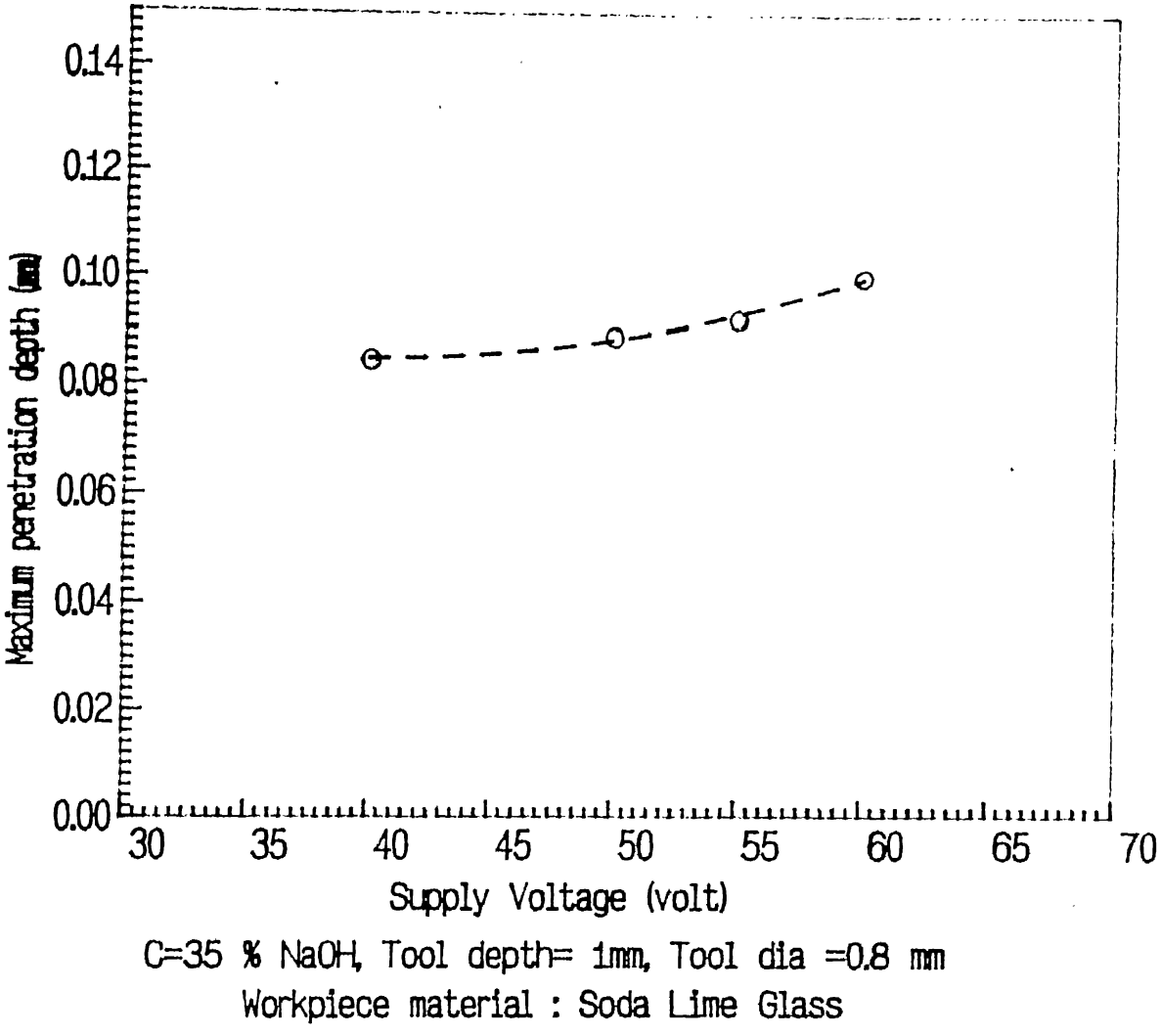

Figure 4.9: Maximum penetration depth Vs Supply Voltage

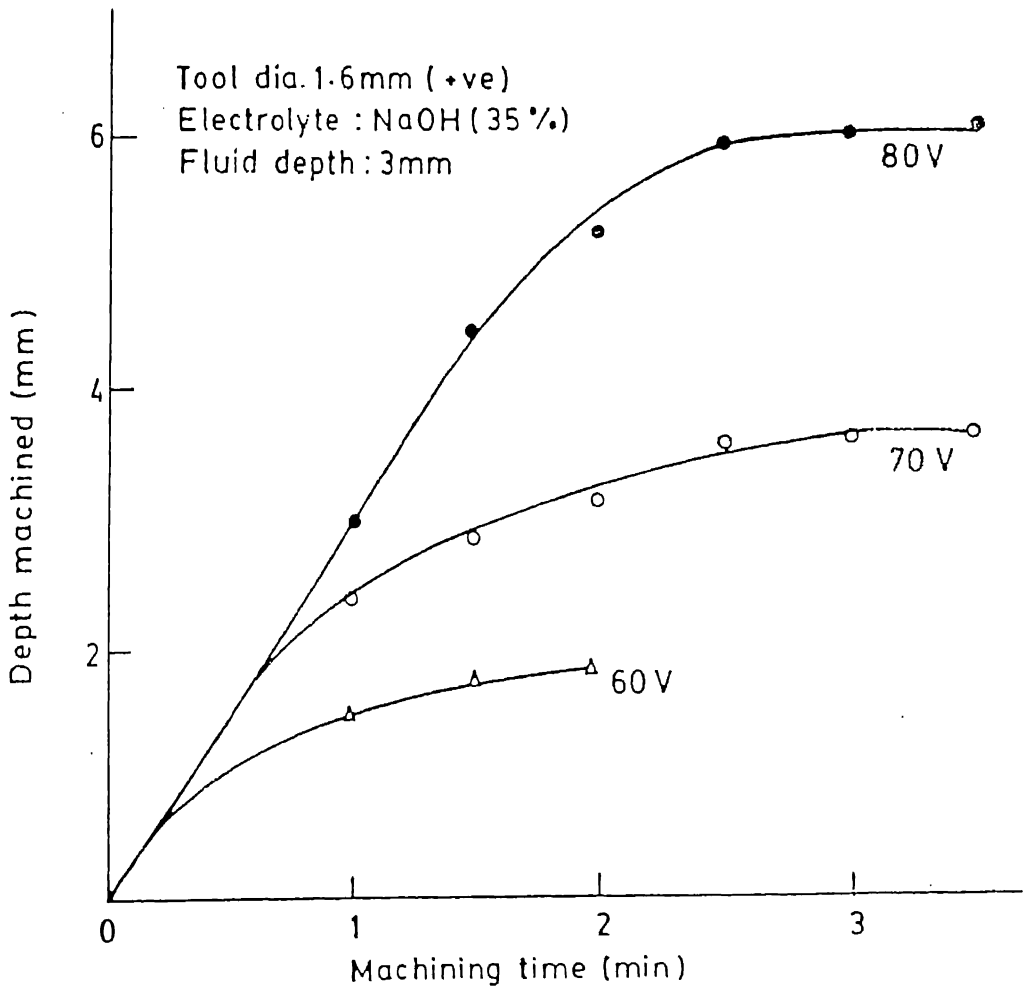

Limited machining depth characteristics
(work material : glass)

Figure 4.10: Maximum penetration depth Vs Supply Voltage (Experimental)

Table 4.1: Comparison of MRR for Borosilicate glass

Experimental MRR mg/min	Theoretical MRR with 0.5% overall machining efficiency
4.4	6.94

reasons :

1. The removed material per spark is proportional to $q^{*1.5}$, where q^* is the heat rate. (This equation has been derived by Basak[2] using analytical method). In the computation the overall machining efficiency (which is the product of thermal and ejection efficiency) has been assumed as 0.5 percent. It is possible that the assumed thermal efficiency is higher than the actual value. In the case, the value of q^* gets overestimated leading to higher MRR.

2. Radiation losses are not taken into consideration.

3. The boundary condition $\frac{\partial T}{\partial n} = 0$ can not be satisfied fully in actual practice. Thus the temperature distribution obtained is always higher than the actual temperature distribution. As a result the computed MRR is slightly more than the actual MRR.

It is reported by researchers [11] that the overall machining efficiency for ECSM process is approximately 1.0 percent. The above results for MRR shows that overall machining efficiency is not constant, but increases with the supply voltage, where overall machining efficiency is defined as ratio of experimentally observed MRR to computed MRR. Figure 4.12 shows the variation of overall efficiency with the supply voltage for the Soda Lime glass. For the case of Borosilicate glass the overall machining efficiency is also of the same order and is 0.317 percent.

4.3 Explanation of Limited Depth Characteristics of the Process

The limited depth characteristics of the ECSM process is a major limitation of the process. The rate of machining in the process is not constant but decreases with the time as indicated

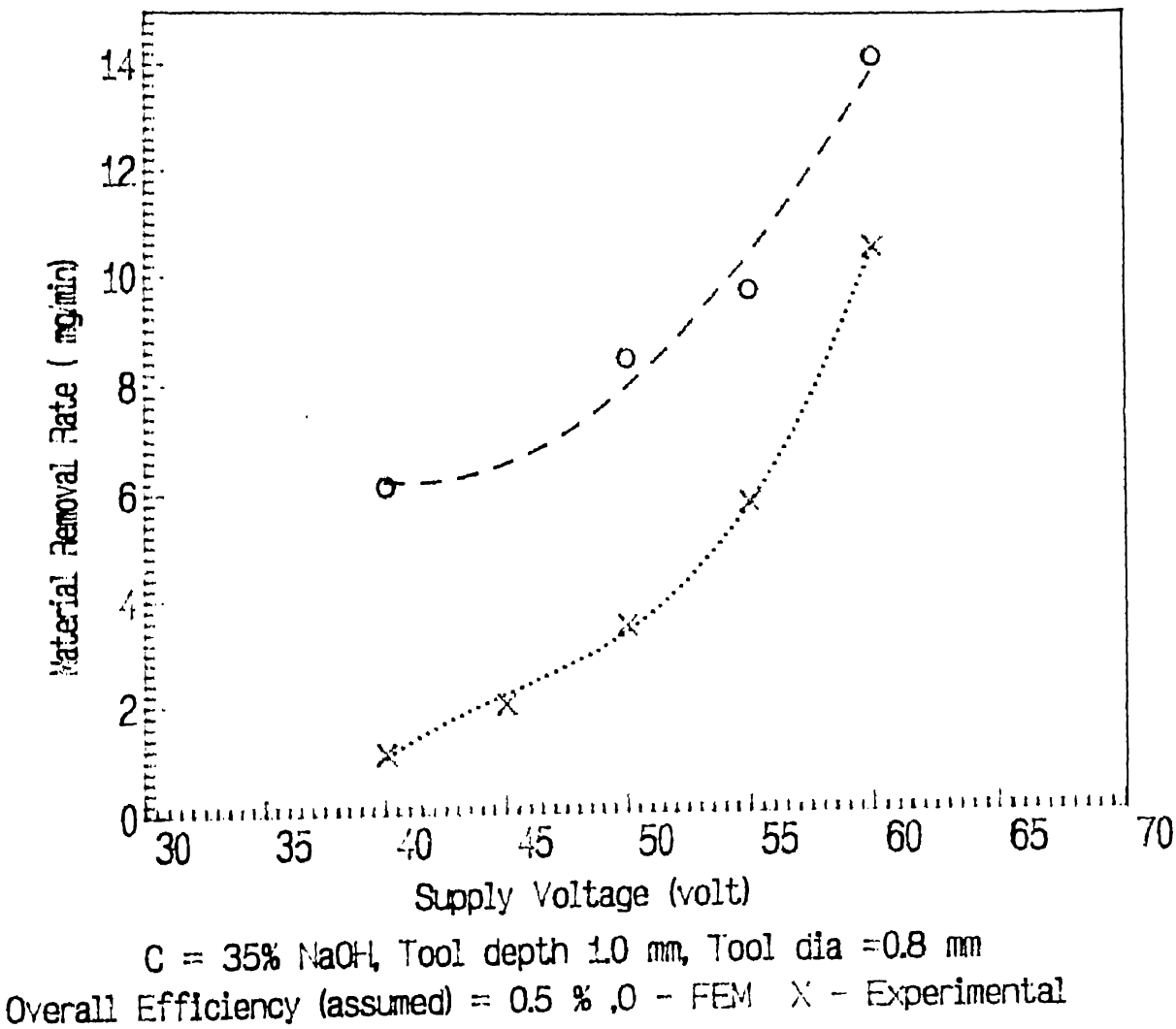

Figure 4.11: Variation of MRR with Supply Voltage for Soda Lime Glass

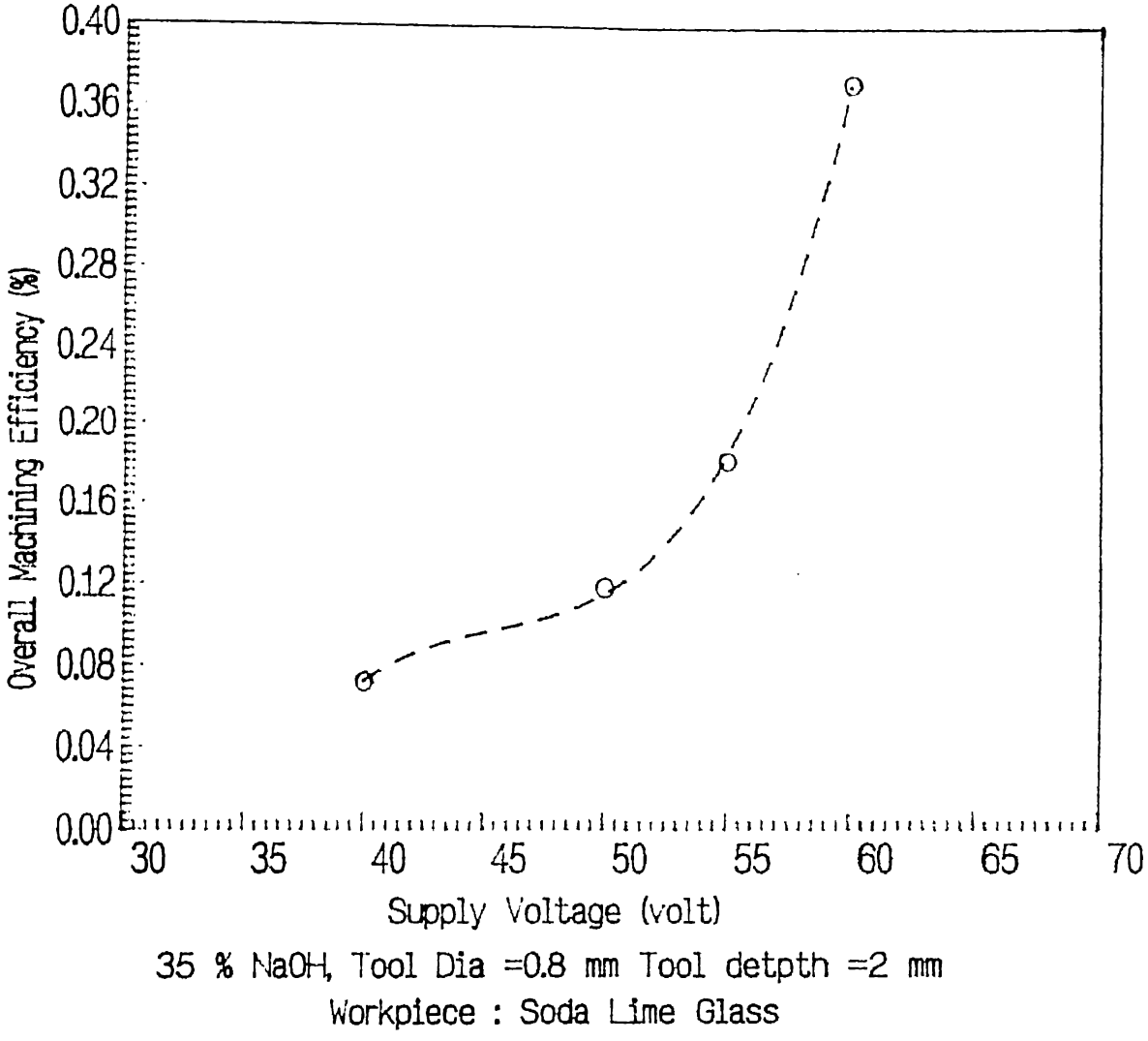

Figure 4.12: Overall Machining Efficiency Vs the Supply voltage

in Figure 4.10. Maximum depth obtained by ECSM process in Soda Lime glass by Cook et al [5] in 1973, is approximately 6.0 mm with 80 volt supply voltage, 35 percent NaOH, 1.6 mm tool diameter (anode is used as tool) in 3 minutes. Recently Gautam [7] drilled hole up to 2.8 mm in Borosilicate glass using eccentrically rotating tool.

The process of lowering of machining rate with the time can be well explained by the help of Isotherm plots. Figure 4.13 shows isotherm plot taken after 10 sparks. The hatched area in the figure shows the softened/removed material after 10 sparks. The isotherm plot shows that there are unmelted part of workpiece material in between.

In ECSM process the location of a spark is governed by the hydrogen bubble across which sparking takes place unlike EDM where minimum distance between tool and workpiece governs the location of the spark. Thus in ECSM process (refer Figure 4.14) there is a possibility that the bubbles are accumulated and grow in the gap formed due to removed material, and there is no sparking near or at the points of unmelted material.

As soon as tool penetrates inside the workpiece the unavailability of the fresh electrolyte in between the tool and workpiece increases which causes lowering of bubble density in between the tool and workpiece, and shifting of the discharge zone takes place.

The above discussion for the limited depth characteristics reveals following possible remedies for the limited depth problem of ECSM -

1. Hollow tool with flowing electrolyte
2. Rotating tool
3. Eccentrically rotating tool
4. Abrasives-Metallic bonded tool
5. Increase in the circuit current by specially designed electrical circuit

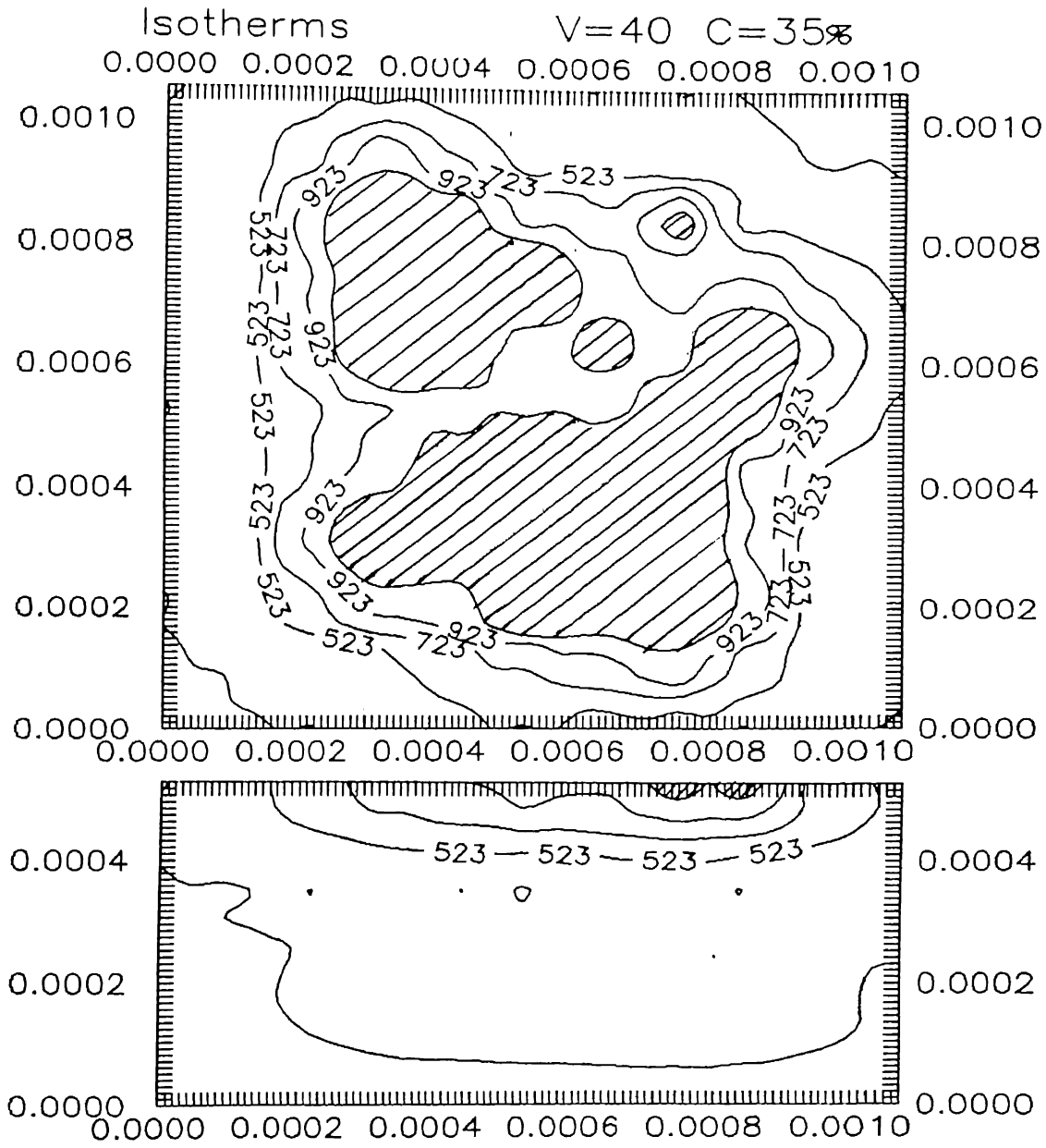

Figure 4.13: Intermediate Isotherms after 10 Sparks

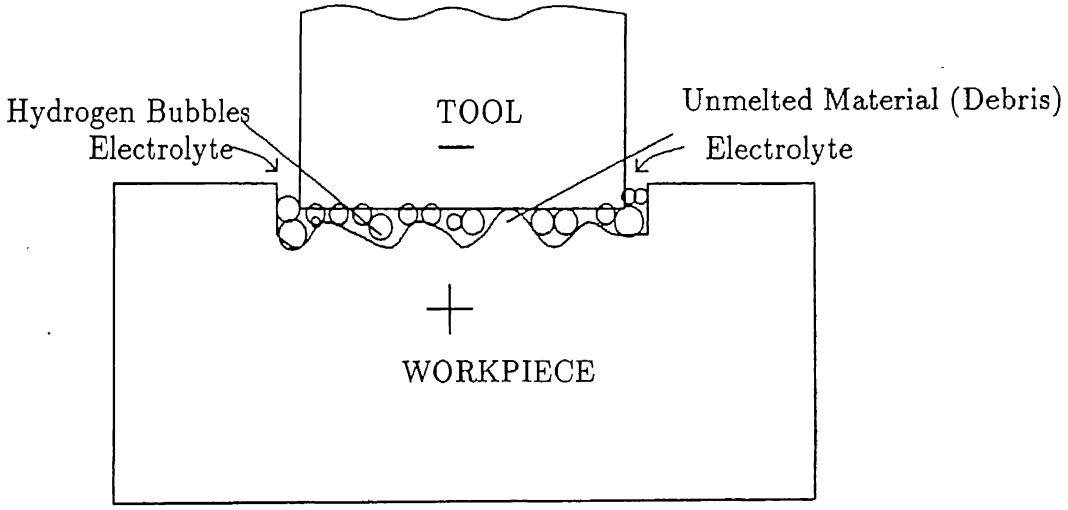

Figure 4.14: Bubble accumulation and effect of debris

Chapter 5

Conclusions and Scope for the Future Work

5.1 Conclusions

Valve theory of ECSM process has been proposed and existing experimental results are explained on the basis of the theory. Expression for circuit current at the time of sparking has been derived by multivariable curve fitting technique, and then it is used for the calculation of spark energy. The discussion also reveals that the proposed arc discharge valve theory of ECSM process is more realistic as compared to switching theory.

An entirely new approach has been proposed for the numerical analysis of the ECSM process which involves 3-D unsteady state heat conduction with random location of heat source (spark). In the actual process the sparks locations are random and thus formulation reaches very near to the actual phenomena. The analysis technique employed is finite element method.

The isotherm plots on the top surface as well as in the depth of workpiece also show a good agreement with the experimental results. The trend of voltage vs MRR curve is similar to the experimental one but the model predicts higher values of MRR as compared to those obtained experimentally.

5.2 Scope for the future work

1. For a better modeling of the process, investigations are needed which may involve observations of the machining zone with the aid of laser photography. The observations would be helpful in explaining the complicated phenomenon, that occurs at machining zone, and thus modeling can be improved.

2. As it is discussed in the previous chapters that process involves many interdependent phenomena. and how these are affecting the material removal rate is still unknown. Thus a model involving fuzzi system approach can give a better picture in such environment of uncertainty.

3. The work can be extended to evaluate produced surfaces by the process.

4. The discharge duration for all discharges is not the same and depends on many factors, mainly on supply voltage, diameters of bubbles, electrolyte concentration etc. A study to evaluate this discharge time experimentally as well as theoretically will be a good contribution for the process.

5. V-I, V-t and I-t characteristics obtained experimentally can throw light on the insight of the ECSM process. It will also help in determining the effect of parameters on the average discharge time.

[13] Kellog H.H.- J of Electrochemical soc, n 97, p 133, 1950

[14] Knight H. B.- The Arc Discharge, Chapman and Hall Ltd, 1960

[15] Kurafuji H., Suda K. - Annal of CIRP, v 16,p 415,1968

[16] Madhu P.- Finite Element Analysis of EDM Process, M.Tech. Thesis, I.I.T. Kanpur,1991

[17] McGeough J. A. - Advanced Methods of Machining, chapman and Hall, 1988

[18] Miller I., Freund J.E. - Probability and Statistics for Engineers Prentice Hall, India, 1981

[19] Nesarikar V. V.,Jain V. K.,Choudhary S. K.- TW-ECSM of thick sheets of Kevlar Epoxy Composites, proc of 16th AIMTDR Conf, p61, 1994

[20] Nicholos P. C.- HandBook of ceremic and composites Mcgrall book company, 1958.

[21] Popular R. - Electrical phenomenon in Gases, Chapman and Hall Ltd, 1963

[22] Rao P. S.- M.Tech Thesis, I.I.T. Kanpur 1988

[23] Reddy J.N.- Introductoin to the Finite element Method, McGraw Hill Book Co,1984

[24] Shand E.B. - Glass Engg Handbook, McGrall book Co, 1958

[25] Shanker P.- Analysis of Spark Discharge in EDM Process, M.Tech. Thesis, I.I.T. Kanpur,1993

[26] Spreabury F.G - Electronics, Sir Issac Pitman and Sons, 1947

[27] Tandon S.- Machining of composites - A new approach, M.Tech. Thesis, I.I.T. Kanpur, 1987

[28] Tsuchiya, Inoue, Miyazak, et al - Bull of Japan Soc of prod engg, v 19,n 1,p 73,1985

[29] TaylorH.- Trans of Electrochemical soc, n 47, p 301, 1925

[30] Umesh Kumar - An experimental study of electrical machining of nonconducting materials, M.Tech. Thesis, I.I.T. Kanpur, 1985

Appendix A

Electrolyte Conductivity Vs percentage Concentration of Electrolyte Solutions[9]

The electrolytic conductivity of NaOH, KOH and NaCl at $18^{o}C$ with the percentage concentration by weight of electrolytes are given in the following figures. The equation for the curves have been obtained by least square curve fitting method.

1. NaOH

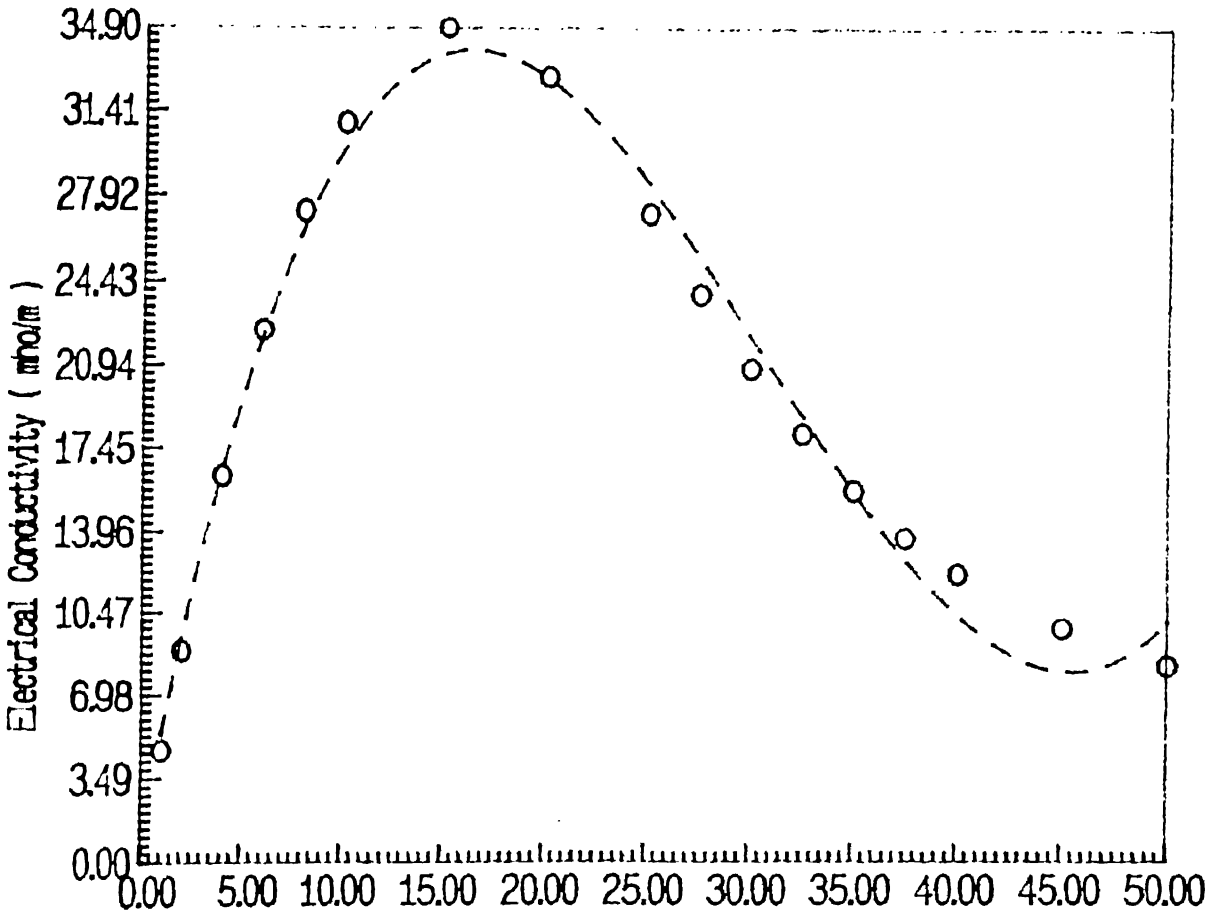

POLYNOMYAL(DEGREE 3)EQUATION IS :

Y = 0.885958+4.62384*X-0.193274*X^2+0.00208907*X^3

2. KOH

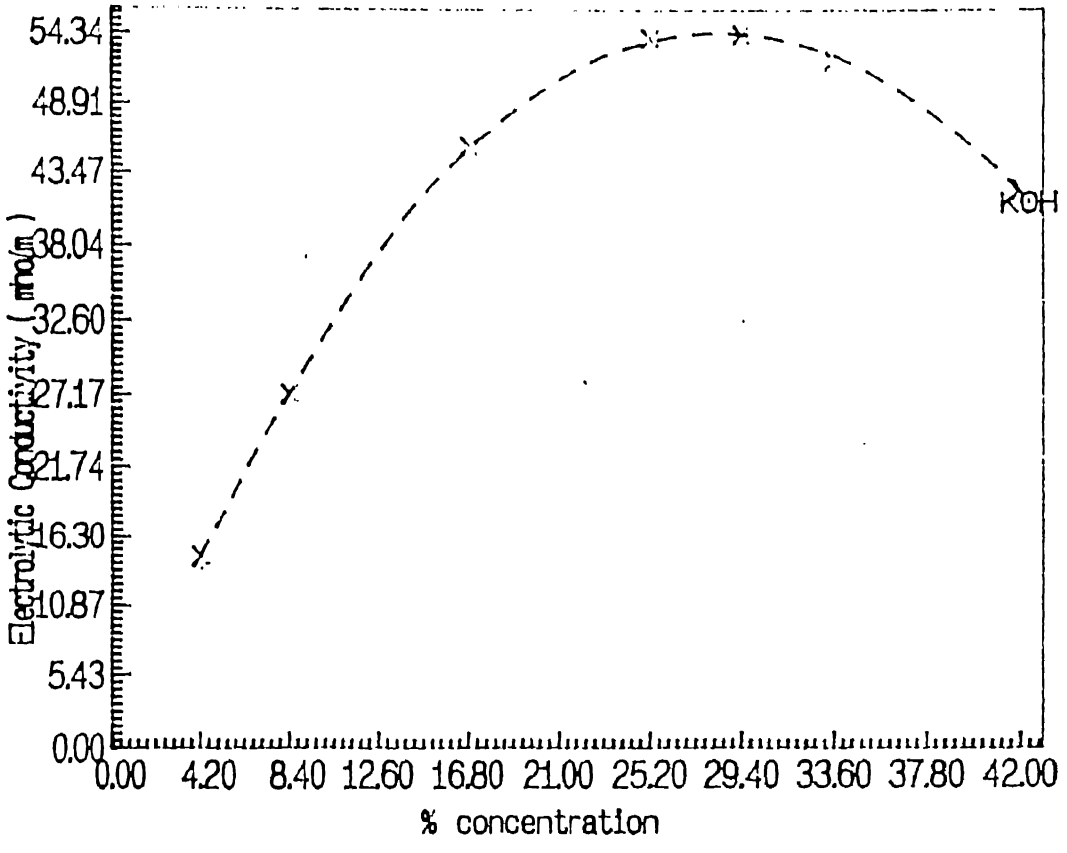

POLYNOMYAL(DEGREE 2)EQUATION IS :

Y = -0.335781+3.86262*X^-0.0680216*X^2

3. NaCl

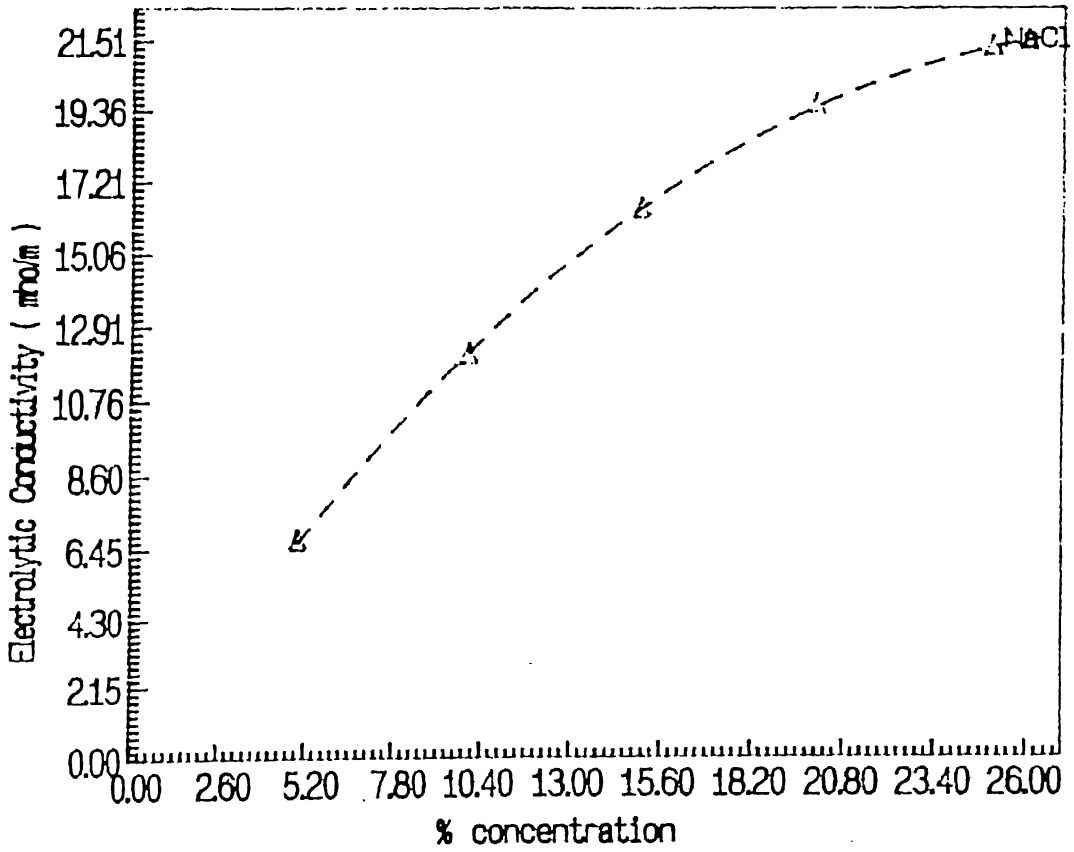

POLYNOMYAL(DEGREE 2)EQUATION IS :

Y = -0.0154902+1.46172*X-0.0243105*X^2

Appendix B

Properties of Workpiece Materials[7,24]

1. Soda Lime Glass

Density = 2500 Kg/cubic m

Softening temperature = 1123 K

Thermal conductivity and specific heat of the soda lime glass are very much dependent on the temperature. Therefore by least square curve fitting method, the equations for the variation in above thermal properties with the temperature are obtained.

Following figures show the variations of thermal conductivity and specific heat of soda lime glass with the temperature :

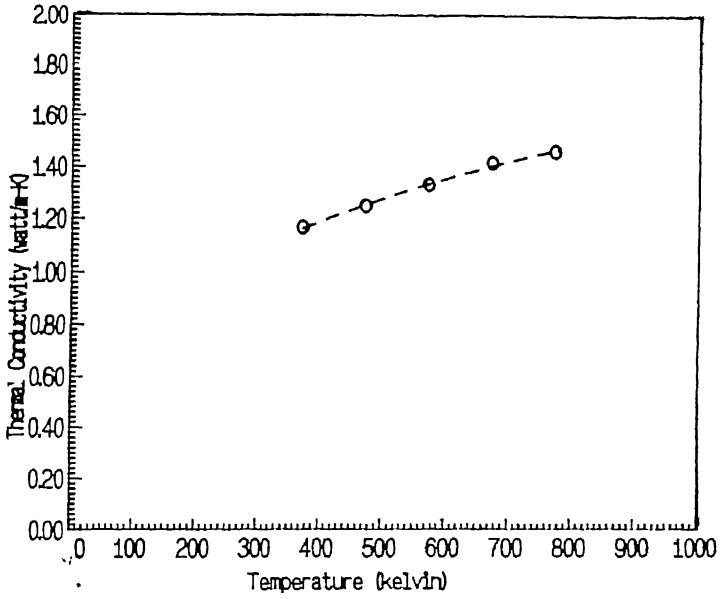

Y = 0.714065+0.00143648*X-5.96931e-07*X^2

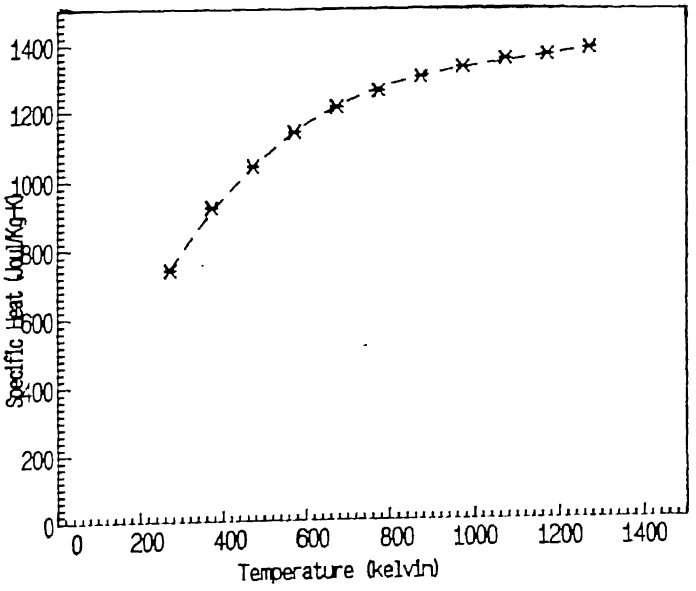

Temperature vs Specific Heat for Soda Lime Glass

Y = 86.9383+3.07447*X-0.00262583*X^2+7.93512e-07*X^3

2. Borosilicate Glass

Density = 2230 Kg/cubic m

Softening temperature = 1093 K

Thermal conductivity and specific heat of the borosilicate glass are also very much dependent on the temperature. Following figures show the variations of thermal conductivity and specific heat of borosilicate glass with the temperature :

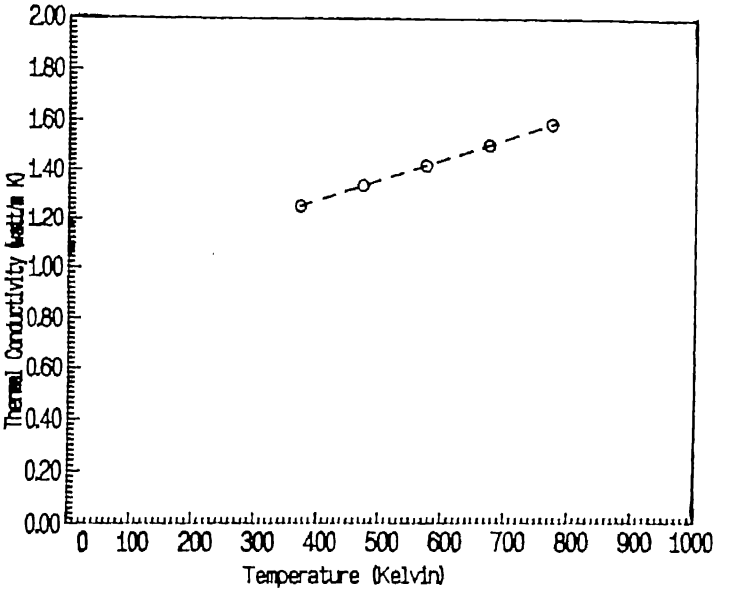

POLYNOMIAL(DEGREE 1)EQUATION IS :

Y = 0.942172+0.000835999*X

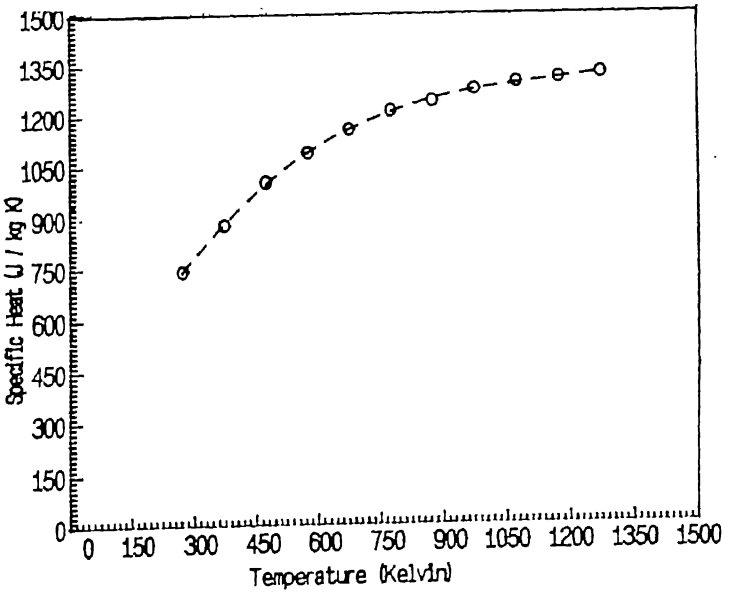

POLYNOMYAL(DEGREE 3)EQUATION IS :

Y = 176.461+2.57864*X-0.00205693*X^2+5.81257e-07*X^3

Calculation of convective heat transfer coefficient

The different physical quantities are considered at the temperature 1100, as 1100 K is considered as mean temperature over the temperature variation range.

Prandtl number

$Pr = \nu/\alpha$

Grashof number

$Gr = \frac{\beta g T_m l^3}{\nu^2}$

$GrPr = 2.974X10^5$

Nusselt number

$Nu = 0.71(GrPr)^{0.25}$ for $10^3 < GrPr < 10^9$

but $Nu = \frac{hl}{K}$

thus

$h = \frac{NuK}{l}$

where

ν = Kinematic viscosity

α = Thermal diffusibility

β = Coefficient of expansion

g = Acceleration due to gravity

T_m= Mean temperature of the wall

l= Characteristics length

h= Convective heat transfer coefficient

K= Thermal conductivity of the medium

The value of the convective heat transfer coefficient is taken as 24870 $watt/m^2K$ in the computations.